The Classic *Lobe* Eye Phenotype of *Drosophila* Is Caused by Transposon Insertion-Induced Misexpression of a Zinc-Finger Transcription Factor

Wonseok Son[1] and Kwang-Wook Choi[2]
Department of Biological Sciences, Korea Advanced Institute of Science and Technology, Daejeon 34141, Korea
ORCID IDs: 0000-0003-1623-1236 (W.S.); 0000-0002-8997-3065 (K.-W.C.)

ABSTRACT *Drosophila Lobe* (*L*) alleles were first discovered ~100 years ago as spontaneous dominant mutants with characteristic developmental eye defects. However, the molecular basis for *L* dominant eye phenotypes has not been clearly understood. A previous work reported identification of *CG10109*/*PRAS40* as the *L* gene, but subsequent analyses suggested that *PRAS40* may not be related to *L*. Here, we revisited the *L* gene to clarify this discrepancy and understand the basis for the dominance of *L* mutations. Genetic analysis localized the *L* gene to *Oaz*, which encodes a homolog of the vertebrate zinc finger protein 423 (Zfp423) family transcriptional regulators. We demonstrate that RNAi knockdown of *Oaz* almost completely restores all *L* dominant alleles tested. $L^{rev6\text{-}3}$, a revertant allele of the L^2 dominant eye phenotype, has an inframe deletion in the *Oaz* coding sequence. Molecular analysis of *L* dominant mutants identified allele-specific insertions of natural transposons (*roo[ ]L*[1], *hopper[ ]L*[5], and *roo[ ]L*[r]) or alterations of a preexisting transposon (L^2-specific mutations in *roo[ ]Mohr*) in the *Oaz* region. In addition, we generated additional L^2-reversion alleles by CRISPR targeting at *Oaz*. These new loss-of-function *Oaz* mutations suppress the dominant *L* eye phenotype. Oaz protein is not expressed in wild-type eye disc but is expressed ectopically in L^2/+ mutant eye disc. We induced male recombination between *Oaz-GAL4* insertions and the L^2 mutation through homologous recombination. By using the L^2-recombined GAL4 reporters, we show that *Oaz-GAL4* is expressed ectopically in L^2 eye imaginal disc. Taken together, our data suggest that neomorphic *L* eye phenotypes are likely due to misregulation of *Oaz* by spontaneous transposon insertions.

KEYWORDS CRISPR; Lobe; natural transposon; Oaz; targeted recombination; Zfp423 family transcriptional factor

It has long been proposed that natural transposons can affect the genome structure and gene regulation in diverse species from plants to humans (Miller and Capy 2004; Maksakova *et al.* 2006; Burns and Boeke 2012). Transposons have conferred important sources for spontaneous mutations and genetic polymorphisms, driving host genome evolution. Transposable elements can be classified into two major groups by transposition mechanisms: DNA transposons and retrotransposons (Bourque *et al.* 2018). In *Drosophila*, DNA transposons such as *P* and *Hopper* elements transpose through a cut-and-paste mechanism. In contrast, retrotransposons like *gypsy* and *opus* are mobilized by a copy-and-paste mechanism. Both groups of natural transposons have been identified abundantly throughout different strains of *Drosophila melanogaster*, composing 10–20% of the whole genome with diverse subgroups (Kaminker *et al.* 2002; Kapitonov and Jurka 2003; Ganko *et al.* 2006).

Studies on several spontaneous mutants have shown that natural transposons can generate loss- or gain-of-function mutations in developmentally important genes by insertions into coding sequences or critical regulatory sequences near the affected genes. For example, *Glazed* (*Gla*) is a dominant mutation that causes defects in eye development. *Gla* turns out to be a gain-of-function allele of the *wingless (wg)* gene, and its eye phenotype results from the Wg misexpression induced by transposon sequences of a *roo* retrotransposon inserted in the *wg* promoter (Brunner *et al.* 1999). Other transposon

doi: https://doi.org/10.1534/genetics.120.303486
Manuscript received August 2, 2019; accepted for publication July 6, 2020; published Early Online July 7, 2020.
Supplemental material available at figshare: https://doi.org/10.25386/genetics.12618950.
[1]Present address: Department of Biological Sciences, Kongju National University, Gongju-si, Chungcheongnam-do 32588, Korea.
[2]Corresponding author: Department of Biological Sciences, Korea Advanced Institute of Science and Technology, 291 Daehak-ro, Yuseong-gu, Daejeon 34141, Korea. E-mail: kchoi100@kaist.ac.kr

sequences can also drive ectopic transcription of different genes to affect eye development in *Drosophila* (Awasaki *et al.* 1996; Mozer 2001). Alternatively, transposons may affect host transcription by altering the chromatin structure around their insertion sites (Morgan *et al.* 1999; Ong-Abdullah *et al.* 2015). Hence, transposable elements provide versatile docking sites for DNA-binding proteins to affect host gene expression (Chuong *et al.* 2017). In this study, we show that several *L* dominant alleles are caused by insertion of transposable elements or modifications of an existing transposable element.

Classical *L* dominant alleles are one of the first *Drosophila* mutants with developmental eye defects. An interesting feature of these eye phenotypes is the preferential reduction in the ventral eye region with variable expressivity depending on genetic backgrounds (Lindsley and Zimm 1992). Genetic interaction studies have shown that *L* eye phenotype can be modified by genetic changes in diverse signaling pathways, including Notch (N), Wg, Decapentaplegic (Dpp), JAK/STAT, and apoptotic pathways (Chern and Choi 2002; Singh *et al.* 2005, 2006; Wang and Huang 2009). However, the molecular nature of the dominant *L* mutations and the basis of these genetic interactions have not been clearly defined.

Previously, we have reported that *L* is an essential gene for viability identified as an uncharacterized *CG10109* (Chern and Choi 2002). *CG10109* turned out to be the *Drosophila* homolog of mammalian PRAS40, a negative regulator of mTOR signaling (Sancak *et al.* 2007; Vander Haar *et al.* 2007). As described in this study, however, subsequent analyses suggested that *L* might be different from *CG10109*. Coincidently, an independent study reported an isolation of a *CG10109/PRAS40* knockout mutant that is viable with no obvious developmental defects (Pallares-Cartes *et al.* 2012). These results led us to reinvestigate the identity of the *L* gene and the molecular lesions of *L* mutant alleles. Here, we show genetic and molecular evidence that *CG42702/Oaz* adjacent to *CG10109/PRAS40* is responsible for *L* mutant eye phenotypes. The *Oaz* gene is a unique *Drosophila* homolog of vertebrate Zfp423 family transcriptional factors containing multiple zinc finger (ZF) motifs. Most vertebrate species have a pair of related genes, *Zfp423* (*OAZ/Ebfaz/ZNF423*) and *Zfp521* (*Evi3/EHZF/ZNF521*), that are involved in diverse developmental processes (Tsai and Reed 1997; Hentges *et al.* 2005; Alcaraz *et al.* 2006; Gupta *et al.* 2010; Kamiya *et al.* 2011; Kiviranta *et al.* 2013). A previous study reported that *Drosophila Oaz* is expressed in the developing and adult brain (Potter and Luo 2010; Hammonds *et al.* 2013), but only a developmental function of the gene has been reported in the embryonic posterior spiracle development (Krattinger *et al.* 2007).

Several classical *L* mutants isolated many decades ago have a common characteristic of dominant eye-specific phenotype. An intriguing question is how spontaneous *L* mutations are related to the dominant small eye phenotype. Evidence suggests that dominant *L* eye phenotypes result from gain-of-function mutations of a gene. For example, the dominant $L^2/+$ eye phenotype was reverted by introduction of loss-of-function mutations like chromosomal deficiencies generated by X-ray irradiation (Baker and Ridge 1980; Davis and MacIntyre 1988). However, the molecular basis underlying the dominant gain-of-function phenotypes of the *L* mutations has been unknown. As described in this study, we have identified natural transposons inserted in the *Oaz* region of spontaneous *L* mutants, implying a possible relationship between the transposon insertions and the *L* eye phenotypes.

Here, we demonstrate that *L* dominant eye phenotypes are restored by reducing *Oaz* expression. We also confirm that *L* dominant eye phenotypes are suppressed by CRISPR targeting of the *Oaz* gene. Finally, we provide evidence that Oaz protein and *Oaz-GAL4* reporter expression are induced ectopically in the mutant eye disc. Taken together, we identify *Oaz* as the *L* gene, and propose that spontaneous transposon insertions or an altered transposon in *Oaz* may drive ectopic *L* expression in the eye disc to cause the gain-of-function eye phenotypes.

Materials and Methods

Drosophila strains

L dominant mutations (L^1, L^2, L^4, L^5, L^r, and L^{si}) and ft^1 were described by Lindsley and Zimm (1992) (Bloomington *Drosophila* Stock Center, BDSC 318, 319, 320, 321, 323, 324, and 304, respectively). $L^{rev6\text{-}3}$ and $PRAS40^{P17}$ were described by Chern and Choi (2002). L^{fee} (Wang and Huang 2009) and $PRAS40^{KO}$ (Pallares-Cartes *et al.* 2012) were obtained from Min-Lang Huang and Aurelio A. Teleman, respectively. Breakpoints of chromosomal deficiencies used for complementation tests (Figure 1A) are described in FlyBase (Thurmond *et al.* 2019) and the following literature: *Df(2R)ED2354* (Ryder *et al.* 2007), *Df(2R)BSC357*, *Df(2R)BSC668*, *Df(2R)BSC700* (Cook *et al.* 2012), *Df(2R)Exel8059*, *Df(2R)BSC11* (Parks *et al.* 2004), *Df(2R)L48* (Davis and MacIntyre 1988), *Df(2R)trix* (Belote and Baker 1987; Lindsley and Zimm 1992), *Df(2R)03072* (Prout *et al.* 1997) (BDSC 8913, 24381, 26520, 26552, 7877, 6455, 6139, 1896, and 5422, respectively). The following RNAi strains and mutants were obtained from BDSC, *Drosophila* Genomics Resource Center (DGRC), Vienna *Drosophila* Resource Center (VDRC), and Harvard Exelixis Collection (Exelixis): *Oaz RNAi* (BDSC 25923, 35715, VDRC v107061), *Oaz-GAL4* (BDSC 30026, DGRC 104937), *Oaz*-EP (BDSC 43537, Exelixis d09084), *PRAS40 RNAi* (VDRC v38338, v38339), *phyl RNAi* (BDSC 29433, VDRC v35469), $phyl^{2245}$ (BDSC 5686, DGRC 108363), $phyl^{2366}$ (BDSC 30723), and *Achl RNAi* (BDSC 25956) (Figure 1B, Figure 2, and Figure 3B).

To minimize genetic background effects on *L* eye phenotypes, *L* alleles and other strains used for genetic tests were backcrossed for 5–10 generations, except for TRiP RNAi strains, which were generated in the isogenic y^1 v^1 or y^1 sc^* v^1 genetic backgrounds and showed consistent effects on *L* dominant alleles. Isogenic control strains of w^{1118} background (Ryder *et al.* 2004) were available from BDSC

(5905, 5906, 5907, 5908). The Cas9 sources (Kondo and Ueda 2013; Port *et al.* 2015) were obtained from BDSC (51323, 54590) and the Fly stock center of the National Institute of Genetics (CAS-0004). The reporter stock of the G-TRACE system (Evans *et al.* 2009) was from BDSC (28280).

Sequencing analyses

Genomic sequences of the region 51A2-4 from *Achl* to *PRAS40* (Figure 1B) were analyzed for *L* alleles (L^1, L^2, L^4, L^5, L^r, L^{si}, L^{fee}, and $L^{rev6\text{-}3}$) and control strains (*CS*, w^{1118}, and ft^1). In the case of $L^{rev6\text{-}3}$, genomic sequences were amplified from heterozygotes between the mutant and the control isogenic second chromosome. Multiple clones were sequenced independently and compared with the corresponding sequences from the progenitor L^2 and the control chromosomes. Transposons in specific *L* alleles were identified by inverse PCR methods. New lethal *L* alleles were generated by CRISPR targeting as described below and sequenced in the same manner as $L^{rev6\text{-}3}$ sequencing.

Generation of PRAS40 RNAi strains

The 501 bp unique *PRAS40* sequence of exon 2 to exon 3 was amplified by PCR, using two primers, 5′-gtgtctcgatggccaggaa gatgtc-3′ and 5′-cagctctctcggccagcgtgg-3′. The amplified fragment was cloned into *pWIZ* (Lee and Carthew 2003) to generate *UAS-PRAS40 RNAi*. Transgenic flies were generated by a standard *Drosophila* germline transformation method (Bachmann and Knust 2008). Transformants were crossed with the ubiquitous *Act-GAL4* driver, and the lines showing no phenotype were selected. The selected lines were able to suppress the phenotype of *PRAS40* overexpression, confirming their RNAi effects.

CRISPR targeting

All guide RNA (gRNA) sequences used are listed in Supplemental Material, Table S1, and the targeting sites in the *L* region are shown by green, red, and orange arrowheads in Figure 5, A and M and Figure S8A.

The initial mutagenesis to isolate L^2-reversion or loss-of-function alleles of *L* followed the protocol of direct microinjection of constructed gRNA vectors (*U6-DM1* or *U6-DM2* in *pBFv-U6.2*) into L^2 or wild-type embryos expressing Cas9 in the germline (*P[nos-Cas9*, y^+, v^+*]*; (Kondo and Ueda 2013) (Figure S1, A and B). L^{DOB} was isolated by the reversion of the $L^2/+$ eye phenotype, and lethal *L* alleles (L^{gR1} and L^{P3}) were collected by screening the F1 progeny based on the failure to complement *Df(2R)ED2354* that uncovers the *L* region. Sequence analyses confirmed specific InDel mutations in those loss-of-function alleles (Figure 5M). Mutagenesis by microinjection of gRNA sources yielded very low mutation rates in the *L* region (<0.1% of >3000 F1 flies screened). Hence, subsequent CRISPR targeting experiments were carried out by using transgenic flies expressing specific gRNA sequences.

The *U6-cbm1* transgenic fly line was generated for *L-RB*-specific mutagenesis using the strategy described by Port *et al.* (2014, 2015). Target sites are indicated by red arrowheads in Figure 5A. L^2 or L^5 mutants carrying the *U6-cbm1* transgene were crossed with a ubiquitous Cas9 source (*M[Act5C-Cas9.P]ZH-2A* or *Act-Cas9* in short), and F1 flies (*Act-Cas9/w* or *Y*; $L^2/+$; *U6-cbm1/+*) were examined for reversion of *L* dominant alleles by somatic targeting (Figure S1C). For germline targeting, L^2 mutants with the gRNA transgene were crossed with flies carrying a germline source of Cas9 (*M[vas-Cas9]ZH-2A*, *vas-Cas9* in short) to collect L^2-reversions by the *L-RB*-specific targeting (Figure S1D). The mutagenic F1 males carrying both transgenes of *Cas9* and *U6-cbm1* were collected (*vas-Cas9/Y*; L^2/*Sco*; *U6-cbm1/+*), and the F2 progeny was screened for modified eye phenotypes. By following the same protocol, the *U6-DE1* transformants that express gRNA sequences flanking *opus[ ]Mohr* were established to excise the transposon from *Mohr* strains. Target sites are indicated by green arrowheads in Figure 5A. The gRNA transgene was also used to induce modification of *L* phenotypes by somatic targeting, or to collect L^2-revertants by targeting the *opus* transposon in the germline of F1 males (*Act-Cas9* or *vas-Cas9/Y*; L^2/*Sco*; *U6-DE1/+*; Figure S1, C and D).

Male recombination between L^2 and Oaz-GAL4 insertions by CRISPR targeting

Using preferential homology-dependent repair (HR) of targeted DNA breaks, we designed targeted recombination between the L^2 mutation and *Oaz-GAL4* insertions (*P[GawB]NP5288* and *P[GawB]GH146*, Figure 4B). The gRNA transgenes, *U6-cbm1* and *U6-csm1* that target distal or proximal sites of *Oaz-GAL4* insertions, respectively (Table S1, target sites are indicated by two pairs of red arrowheads in Figure S8A), were used to induce male recombination between L^2 and *Oaz-GAL4* chromosomes. For the targeted recombination, mutagenic F1 males of *vas-Cas9/Y*; L^2/*Oaz-GAL4*; *U6-cbm1* (or *U6-csm1*)/+ were constructed and were crossed with *CyO* balancer females (Figure S1E). F2 progeny flies were screened for recombinants that show both dominant traits of parental or modified $L^2/+$ eye phenotypes and *mini-white* (w^{+m}) expression by *Oaz-GAL4* insertions, and then recombined sequences around target sites were determined (Figure S8).

Immunohistochemistry

An anti-L antiserum was generated by using the C-terminal part of Oaz product (corresponding to G^{768} to the last A^{1228} of L-PB, including eight ZF motifs) that was expressed as a fusion protein with GST, and collected from rats after a series of subcutaneous injections of the purified fusion protein. Immunohistochemistry was performed using the staining protocol described in Patel (1994) with a modification of blocking solution (0.3 M NaCl, 1% NP-40, 0.5% BSA, and 10% NGS) for the more stringent condition. Binding solutions containing the anti-L antiserum were pretreated overnight with fixed w^{1118} embryos at 2 hr after egg laying (AEL) before primary staining of sample embryos, or were pretreated with fixed embryos and first instar larvae at 24 hr AEL before

staining of larval imaginal discs. Fixed embryos were prepared in the whole-mount preparation procedure described in Patel (1994), and larval tissues including imaginal discs were fixed as described in Spratford and Kumar (2014). Those fixed samples were incubated for 2 hr to overnight at 4° in the aforesaid pretreated binding solutions containing primary antibodies, and were then treated with fluorescent secondary antibodies in a standard binding solution (PBS of 175 mM NaCl, 0.5% Tween-20, and 0.1% BSA) for 1–2 hr at room temperature (RT). After washing over 2 hr at RT and/or overnight at 4° in PBS with 1% Tween-20, samples were mounted in Vectashield with DAPI (Vector Laboratories). Fluorescent images were acquired using ZEISS LSM710 and LSM780 microscope systems.

Data availability

Strains and plasmids are available upon request. The authors affirm that all data necessary for confirming the conclusions of the article are present within the article, figures, and tables. Supplemental material available at figshare: https://doi.org/10.25386/genetics.12618950.

Results

Lobe is independent of CG10109/PRAS40

A *P*-element insertion (*P17*) allele was isolated in a previous study as a lethal mutation that enhanced L^{si}/+ eye phenotype. *P17* was an insertion within the *CG10109* gene (labeled as $P[PZ]PRAS40^{P17}$ in Figure 1B; Chern and Choi 2002). In subsequent genetic analyses, however, *P17* could complement a semi-lethal allele $L^{rev6\text{-}3}$, which was isolated as a revertant suppressor of L^2 dominant allele. Further tests also indicated that these two mutations are not allelic. While $L^{rev6\text{-}3}$ was lethal over *Df(2R)L48* (Figure 1A), which is a revertant deficiency isolated as a suppressor of L^2 eye phenotype (Davis and MacIntyre 1988), the lethal *P17* mutation complemented the *L* deficiency as well as $L^{rev6\text{-}3}$.

To test whether the *P17 P*-element insertion is responsible for the lethality, this *P*-element was mobilized to generate revertants by precise excision. However, no viable revertant was found from over 200 independent jumping events. Subsequently, we were able to remove the lethality by backcrossing with an isogenic control strain (Ryder *et al.* 2004). Viable *P17* homozygous flies developed normally without any visible phenotype in the eye (Figure S2B), which is consistent with the report that a knockout allele of *CG10109/PRAS40* generated by homologous recombination is fully viable with no detectable developmental defects (Pallares-Cartes *et al.* 2012). Taken together, these results indicate that the *P17* insertion in *CG10109* is not lethal. *P17* seems to be an amorphic or strong hypomorphic allele of *CG10109* since CG10109 protein was nearly undetectable in *P17* mutant clones generated in eye discs (Figure S2, C and D). Furthermore, the dominant L^2/+ eye phenotypes were not modified by the isogenized *P17*/+ or $PRAS40^{KO}$/+ (Figure S2, J and L), supporting that the *L* eye phenotype is independent of the *P17* insertion.

$L^{rev6\text{-}3}$ lethality maps to Oaz

Previous studies had mapped the *L* gene to the 51A2-B1 region by breakpoints of a *L*-revertant deficiency, *Df(2R)L4* (Baker and Ridge 1980). Since $L^{rev6\text{-}3}$ is a semilethal mutation that suppresses L^2/+ dominant eye phenotypes, probably due to an intragenic mutation, we tried to map the recessive lethality of $L^{rev6\text{-}3}$. To identify the gene for $L^{rev6\text{-}3}$, we carried out complementation tests between $L^{rev6\text{-}3}$ and several deficiency chromosomes that uncover a region of 50E–51E (Figure 1A). $L^{rev6\text{-}3}$, which shows 0–5% survival of homozygous adult flies depending on culture conditions, was clearly lethal when heterozygous for deficiencies such as *Df(2R)ED2354*, *Df(2R)BSC357*, *Df(2R)BSC668*, *Df(2R)BSC11*, and *Df(2R)trix*, as well as *Df(2R)L48*. In contrast, two other deficiencies, *Df(2R)BSC700* and *Df(2R)Exel8059*, complemented the $L^{rev6\text{-}3}$ lethality (Figure 1A). These tests with deficiencies mapped the $L^{rev6\text{-}3}$ lethality within a chromosomal region between 51A2 and 51A4, from the distal breakpoint of *Df(2R)BSC700* to the proximal breakpoint of *Df(2R)Exel8059*. In this region, four coding genes have been annotated: *Achilles* (*Achl*), *phyllopod* (*phyl*), *Oaz*, and *CG10109/PRAS40* (Figure 1B). From this list, we eliminated *Achl* and *phyl* because these genes are intact in *Df(2R)BSC668*, which failed to complement $L^{rev6\text{-}3}$. Thus, the lethality of $L^{rev6\text{-}3}$ might map to either *Oaz* or *PRAS40*. However, since no sequence difference was detected between L^2 and its revertant $L^{rev6\text{-}3}$ in the *PRAS40* genomic region, it is likely that the lethality of $L^{rev6\text{-}3}$ maps to *Oaz*.

Reduced Oaz suppresses L dominant eye phenotypes

Although $L^{rev6\text{-}3}$ lethality was mapped to *Oaz*, it remained to be determined whether the dominant *L* eye phenotype maps to the same gene. Based on the suppression of *L* phenotypes by *L* deficiencies (Baker and Ridge 1980; Davis and MacIntyre 1988), we reasoned that the eye phenotypes of *L* dominant mutations (L^1, L^2, L^5, and L^{si}; Figure 2) might be suppressed by reduced expression of those four candidate genes located between 51A2 and 51A4 (*Achl*, *phyl*, *Oaz*, and *PRAS40*, Figure 1B). L^1 and L^{si} are weak dominant alleles that usually show small dentation in the anterior edge of heterozygous mutant eyes. Comparison of *L* dominant phenotypes in heterozygous flies indicates that L^5/+ is much stronger than L^1/+ and L^{si}/+, but milder than L^2/+ which is the strongest *L* allele. Because *L* eye phenotypes are highly variable depending on the genetic background, those *L* mutant alleles were backcrossed for 10 generations to minimize the potential effects of nonspecific genetic background. We then tested whether these *L* eye phenotypes can be modified by RNAi knockdown of the four candidate genes in developing eye discs using *ey-GAL4*-driven UAS-dsRNA expression.

First, we checked for genetic interaction between *PRAS40* and *L* mutants. Two RNAi strains against *PRAS40*, *P[GD6869]v38338* and *P[GD6869]v38339*, could fully restore the small eye phenotype caused by *PRAS40* overexpression

(hereafter *ey* > *PRAS40*). However, no significant modification of dominant *L* eyes was seen with these *PRAS40* RNAi lines. Since both *PRAS40* RNAi lines showed off-target lethality when expressed ubiquitously with *Act-GAL4* or *Tub-GAL4*, we generated new transgenic RNAi lines by targeting more unique sequences in the *PRAS40* 3′ coding region (*Materials and Methods*). This new *PRAS40* RNAi line did not cause any noticeable developmental defects with *Act-GAL4*, but strongly suppressed the *ey* > *PRAS40* phenotype (Figure S2, E and G), while *P17/+* could partially suppress the phenotype (Figure S2, E and F). These results indicate that this new RNAi line efficiently knocked down *PRAS40*. However, the new *PRAS40* RNAi still could not modify L^2/+ dominant eye phenotype (Figure 2J).

Next, we tested whether *phyl* and *Achl* genetically interact with *L* mutations. Two independent *phyl* RNAi strains (*P[TRiP.JF03369]* and *P[GD12579]v35469*) failed to modify *L* phenotypes (Figure 2I). In addition, two lethal deletion mutants of *phyl*, $phyl^{2245}$/+ and $phyl^{2366}$/+ (Chang *et al.* 1995), did not show any genetic interaction with $L^{rev6\text{-}3}$ or *L* dominant mutants. Three *P*-element insertions have been reported in the promoter region of *Achl* (Thurmond *et al.* 2019). One of them, *P[GawB]NP4297*, was initially lethal and greatly enhanced *L* eye phenotypes. However, after several generations of backcrossing, this *P*-element insertion line became viable and was unable to modify *L* phenotypes. Only one TRiP RNAi strain of *Achl* (*P[TRiP.JF01976]*) was available, and this RNAi also did not noticeably modify the L^2/+ eye phenotypes (Figure 2H).

Finally, we checked whether *Oaz* shows any genetic interaction with the dominant *L* alleles. Strikingly, *Oaz* RNAi (*P[TRiP.GLV21080]*) showed strong suppression of the L^2/+ eye phenotype to the normal eye and consistently rescued all tested dominant mutant *L* phenotypes (Figure 2, K, N, P, and R). Two other independent *Oaz* RNAi lines (*P[TRiP.JF01943]* and *P[KK102438]*) also resulted in weaker but significant suppression of L^2/+ eye (Figure 2L). Taken together, these data suggest that *L* dominant eye phenotypes are caused by abnormal upregulation or ectopic expression of *Oaz*.

To see whether overexpression of *Oaz* can induce the *L* mutant phenotype, we used EP lines (*P[XP]d09084* and *P[GSV1]s-72*) that have UAS elements in the upstream of *Oaz-RB* sequence (Thibault *et al.* 2004; Kankel *et al.* 2007; Cruz *et al.* 2009). When those EP lines were combined with *ey-GAL4* to overexpress *Oaz* in developing eyes, resultant flies showed variable but distinctive eye defects that are similar to that of *L* dominant alleles (Figure S3, A–D). This further supports the idea that the gain-of-function of *Oaz* is sufficient to induce the *L* eye phenotype.

$L^{rev6\text{-}3}$ mutant has a deletion in the Oaz coding region

As shown earlier, the lethality of $L^{rev6\text{-}3}$ was mapped to the 51A2-4 region (Figure 1). To identify the molecular lesion of this potential loss-of-function allele of *L*, we carried out sequence analysis in the 51A2-4 region from *Achl* to *PRAS40*, and compared the sequences between $L^{rev6\text{-}3}$ and its progenitor L^2. As described above, no sequence difference was found between L^2 and $L^{rev6\text{-}3}$ in the *PRAS40* genomic region. Genomic sequences around *phyl* and *Achl* were also identical between the two mutants. However, a small deletion of six amino acid residues was found in the *Oaz* coding sequence of $L^{rev6\text{-}3}$ (Figure 3 and Figure 4B), which corresponds to a putative Mad-binding ZF motif of the Oaz protein (Hata *et al.* 2000; Krattinger *et al.* 2007). Since this deletion was found only in $L^{rev6\text{-}3}$ but not in the progenitor L^2, this deletion is likely to be the specific $L^{rev6\text{-}3}$ mutation that suppresses the dominant L^2 eye phenotype. Since transheterozygotes of $L^{rev6\text{-}3}$ over *L* deficiencies uncovering *Oaz* are lethal, *Oaz* is an essential gene and $L^{rev6\text{-}3}$ might be a loss-of-function allele of *Oaz*.

Based on these genetic and molecular data described above, we conclude that *Oaz* is the responsible gene for $L^{rev6\text{-}3}$ mutation and dominant *L* eye phenotypes. In accordance with the FlyBase guidelines for nomenclature (https://wiki.flybase.org/wiki/FlyBase:Nomenclature) (Thurmond *et al.* 2019), we propose to rename *Oaz* as *L* since *L* was named earlier based on the mutant phenotypes. Accordingly, *Oaz* will be referred to hereafter as *L*.

L dominant alleles contain transposable elements in the *L* region

Next, we examined genomic sequences from *L* dominant alleles to identify molecular lesions for the mutant eye phenotypes. All *L* dominant alleles are spontaneous mutations isolated many decades ago (Lindsley and Zimm 1992; Wang and Huang 2009). When compared with wild-type control sequences of w^{1118} or *CS*, *L* mutants showed a number of polymorphisms in genomic DNA sequences and in deduced amino acid sequences of the four candidate genes in the 51A2-4 region (Figure 3B). Remarkably, however, all four *L* alleles (L^1, L^2, L^5, and L^r) showed almost identical sequences in the genomic region.

These *L* dominant mutants were isolated in a similar time period ~1920 (Lindsley and Zimm 1992). Thus, we looked for a non-*L* mutant isolated during this time period, assuming that such a mutant might have a similar genetic background as *L* mutants. Indeed, the ft^1 mutant chromosome isolated by Mohr (Lindsley and Zimm 1992) showed almost identical sequences to the *L* mutants in the examined genomic region, hence providing control for sequence comparison with the *L* alleles. Analysis of the genomic region 51A2-4 from ft^1 and the four *L* dominant mutants (hereafter referred to as the "*Mohr* strains" after the discoverer's name) showed interesting sequence differences only in the *L* region.

The *L* gene region comprises >30 kb-long sequences within which two different splice forms of *L* (*L-RB* and *L-RC*) have been predicted (FlyBase, GBrowse release 5.57; Figure 4), although only the *L-RB* form was reported (Krattinger *et al.* 2007). We confirmed the expression of both forms by RT-PCR from Canton-S wild-type embryos (Figure S4A). Thus, we examined the entire *L* region including the long intron sequences around *L-RC* exons to identify

molecular lesions in *L* mutants. The *Mohr* strains shared insertions of two different transposons around the second exon of *L-RC*. One was a partial sequence (369 bp) of *jockey* transposon located just before the exon 2 (*jockey[ ]Mohr* in Figure 4A), and the other was an expanded form of *opus* transposon just after the exon 2 (*opus[ ]Mohr* in Figure 4A). The typical *opus* transposon is known to be 7.6 kb long. We confirmed the presence of ~6 kb canonical border sequences of the *opus[ ]Mohr*, but the more interior region of the transposon could not be amplified by PCR for sequencing, possibly due to additional transposon insertions within the *opus* element. However, this *opus[ ]Mohr* was also found in the ft^1 control mutant, suggesting that this transposon is probably not related to the dominant *L* phenotypes.

Interestingly, among *Mohr* strains, L^1 has a specific *roo* transposon insertion in the first *L-RB* intron, located ~1.2 kb downstream from the *L-RB* transcription initiation (*roo[ ]*L^1 in Figure 4B). Furthermore, another specific *roo* element was found in the L^r mutant in the second intron of *L-RC* (*roo[ ]*L^r in Figure 4B). These *roo* elements were not detected in the ft^1 sequence, thus the transposon insertions might be the cause of gain-of-function phenotypes of L^1 and L^r mutants. In addition to the *roo* element insertions, we found that L^5 has a 1.4 kb *hopper* transposon in the first intron of *L-RC* (*hopper[ ]*L^5 in Figure 4B).

L^2 allele shows alterations in the roo[ ]Mohr transposon

The L^2 mutation causes the strongest eye phenotype among classical *L* dominant mutations. However, we could not find any molecular difference between L^2 and the control ft^1 within the sequenced region of *L* transcription. Hence, we examined whether L^2 mutation might be located in the 5′ or 3′ intergenic region. We found that all *Mohr* strains share an intact *roo* element in the 3′ intergenic region (Figure 4, A and C). This *roo* insertion is different from *roo[ ]828* described in the FlyBase reference genome (GBrowse release 5.57). *roo[ ]828* was not detected in all examined stocks including w^{1118} and *CS* controls, as reported in a previous study (Potter and Luo 2010). The *roo* element found in the *Mohr* strains, labeled as *roo[ ]Mohr*, is positioned at 261 bp proximal to the *roo[ ]828* insertion, and is ~1.9 and 5.4 kb away from the *L* stop codon and the first exon of *PRAS40*, respectively. This 9088-bp-long *roo[ ]Mohr* contained a conserved intact long ORF of the *roo* long terminal repeats (LTR) retrotransposon.

Interestingly, we found that the ORF of *roo[ ]Mohr* in L^2 mutant has specific sequence alterations such as a 622 bp duplication, a 5 bp deletion, and a nucleotide change (Figure 4C). Because no other sequence difference was found between L^2 and the control ft^1 within the genomic region from *phyl* to *PRAS40*, the L^2-specific *roo[ ]Mohr* is likely to be the cause of $L^2/+$ eye phenotype that can be suppressed by *L* knockdown (Figure 2).

New L^2-revertants or loss-of-function L alleles fail to complement $L^{rev6\text{-}3}$ lethality

To substantiate the postulation that the $L^{rev6\text{-}3}$ small deletion is responsible for the reversion of the L^2 eye phenotype, we generated new L^2-reverting mutations by specific CRISPR mutagenesis that targets the coding sequence of the *L* gene. The CRISPR target was chosen to cover the coding sequence deleted in $L^{rev6\text{-}3}$ (Figure 5, A and M, orange arrowheads). L^2 embryos expressing Cas9 in the germline (L^2/*CyO*, *nos-Cas9*) were injected with a gRNA construct described in *Materials and Methods*. From F2 progeny, we isolated a new mutant L^{D0B} that reverted the $L^2/+$ eye phenotype (Figure 5F). In the isogenized $L^{rev6\text{-}3}$ heterozygote population (w^{1118}; $L^{rev6\text{-}3}/+$), ~40–80% of flies ($n > 1000$) showed weak eye phenotypes such as small dents in the anterior part of the eye (Figure 5E) similarly to L^1 (Figure 5B). In contrast, most $L^{D0B}/+$ flies had nearly wild-type eyes. Occasionally, $L^{D0B}/+$ eyes showed weak *L* phenotypes but at a significantly lower rate than $L^{rev6\text{-}3}/+$ (<10%, $n > 1000$), suggesting that L^{DOB} is a stronger allele than $L^{rev6\text{-}3}$ (Figure 5F, as compared to Figure 5E). Molecular analysis of L^{D0B} indicated that a codon corresponding to A^{600} of L-PB was replaced with insertion of extra eight nucleotides. This change causes a frame-shift that results in an early translation termination after 29 aberrant codons, thus deleting more than half of the C-terminal L product, including 12 out of 21 ZF motifs (Figure 5M). These molecular data are consistent with the stronger reversion of the $L^2/+$ eye phenotype by L^{D0B} than $L^{rev6\text{-}3}$. We also confirmed that L^{D0B} could not complement the lethality of $L^{rev6\text{-}3}$ and deficiencies uncovering *L* region, such as *Df(2R)ED2354*, *Df(2R)BSC357*, *Df(2R)BSC668*, *Df(2R)BSC11*, and *Df(2R)L48* (Figure 1A). Hence, L^{DOB} mutation is allelic to $L^{rev6\text{-}3}$.

L revertant mutations like $L^{rev6\text{-}3}$ were made in the L^2 mutant background. To generate specific *L* loss-of-function mutations without L^2 dominant mutation, we carried out an additional CRISPR mutagenesis in the wild-type background. By the same CRISPR strategy used for isolating L^{D0B}, we targeted a further upstream site marked by the left arrowhead in Figure 5M. We obtained two lethal alleles, L^{gR1} and L^{P3} (Figure 5, G and H), that show 10- and 11-bp deletion in the last exon of *L*, respectively. These mutations result in frame-shifts after A^{268} and A^{269} of the L-PB product, respectively, thus removing most part of Zn-finger motifs of L protein (Figure 5M). Both of these mutations are allelic to *L* as they failed to complement the lethality of L^2-revertant mutations ($L^{rev6\text{-}3}$ and L^{D0B}) and deficiencies uncovering the *L* gene. Thus, L^2-reverting mutations such as $L^{rev6\text{-}3}$ and L^{D0B} are loss-of-function mutations in *L*, different from classical *L* gain-of-function alleles that are viable as transheterozygotes with *L* deficiencies (Figure 5, B–D). Our data also support that the reversion of the $L^2/+$ eye phenotype by $L^{rev6\text{-}3}$ is attributed to the small deletion in the coding region of *L*.

It has been reported that *L* has a role in the development of the posterior spiracle in the embryo (Krattinger *et al.* 2007). By *L-GAL4* expression (*P[GawB]NP5288* and *P[GawB]GH146* in Figure 4B), we found *L* expression in embryonic or larval posterior spiracles (Figure S7C and S9A). We also checked whether $L^{rev6\text{-}3}$ and newly isolated lethal *L* mutants exhibit any defects in the posterior spiracle development. The majority of L^{gR1} homozygotes could not complete

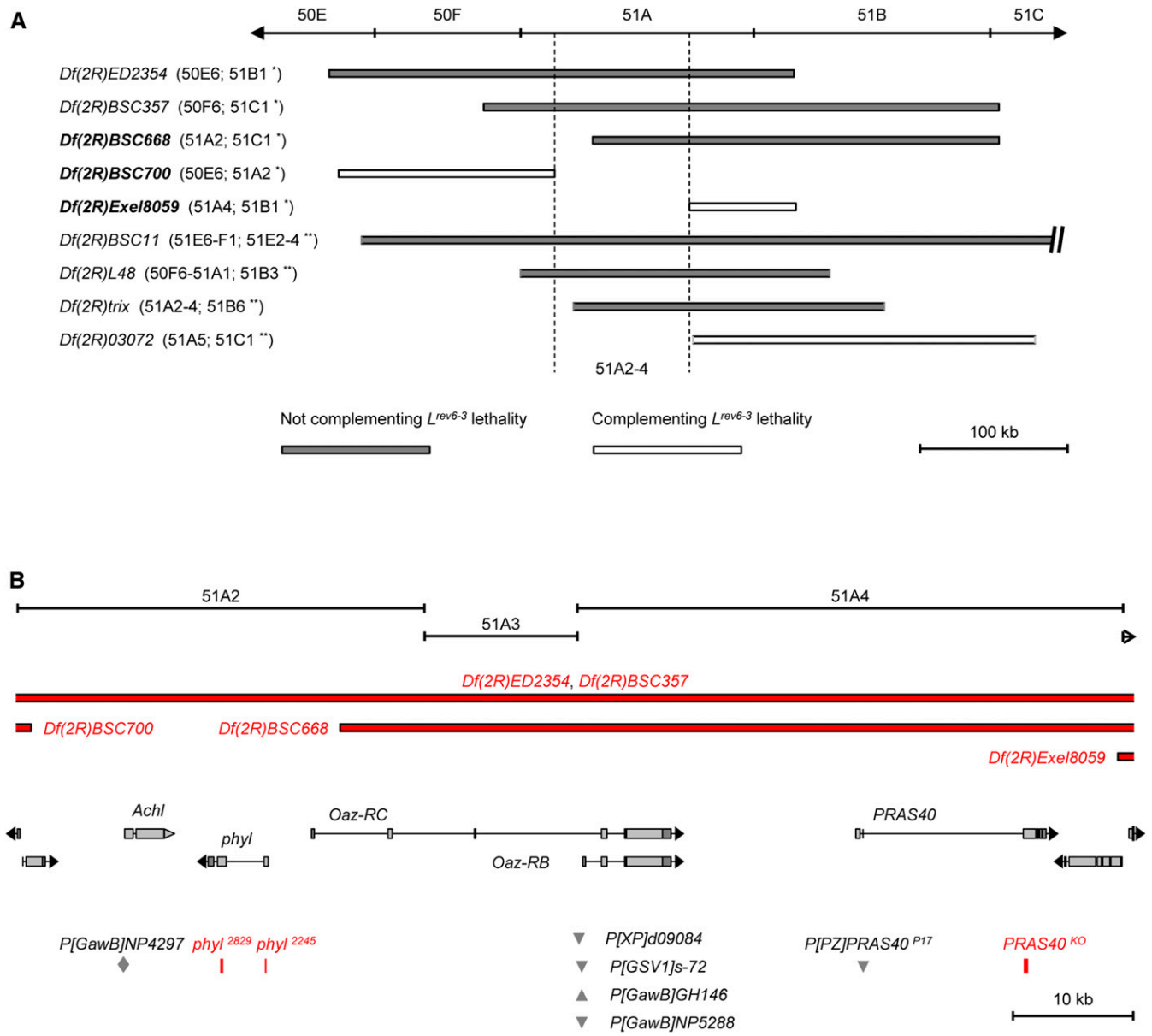

Figure 1 Genomic map around *L/Oaz* gene and localization of $L^{rev6\text{-}3}$ lethality. (A) Deficiency chromosomes used in complementation tests. The $L^{rev6\text{-}3}$ lethality was mapped within the genomic region of 51A2-4 from the distal breakpoint of *Df(2R)BSC700* to the proximal breakpoint of *Df(2R)Exel8059*. A single asterisk (*) indicates that breakpoints were confirmed by sequencing analyses, or predicted by the insertion sites of progenitor P-elements (Parks *et al.* 2004; Ryder *et al.* 2007; Cook *et al.* 2012). The double asterisk (**) indicates the breakpoints determined from polytene chromosome analyses and/or genetic mapping. (B) In the genomic region of 51A2-4, four candidate genes of predicted ORFs were identified; *Achl*, *phyl*, *L/Oaz*, and *PRAS40* (adapted from the FlyBase Genome Browser). Deficiencies of molecularly defined breakpoints are shown by thick red lines (*Df(2R)ED2354*, *Df(2R)BSC357*, *Df(2R)BSC668*, *Df(2R)BSC700*, and *Df(2R)Exel8059*). Gray triangles indicate P-element insertions in candidate genes. Red bars are small deletions. $P[PZ]PRAS40^{P17}$ is the *P17* insertion (Chern and Choi 2002).

embryogenesis, although 0–5% of embryos hatched and died as first instar larvae. In contrast to $L^{gR1}/+$ heterozygotes that show the normal pattern of posterior spiracles, homozygous larvae showed reduced and malformed posterior structures (Figure S5B). Similar defects were also found in L^{P3} homozygous larvae or in transheterozygotes of $L^{rev6\text{-}3}$ with L^{gR1} or L^{P3} mutations (Figure S5, C–G). Consistent with *L-GAL4* expression in posterior spiracles, these data suggest that all new *L* mutations affect posterior spiracle development.

L-RB-specific mutations suppress L²/+ eye phenotype and causes lethality

As described above, we confirmed that two splice forms of the *L* gene, *L-RB* and *L-RC*, are expressed (Figure S4A). We also showed that ectopic expression of *L-RB* by two EP elements (*P[XP]d9084* and *P[GSV1]s-72*, Figure 4B) inserted upstream to the *L-RB* transcription can cause dominant *L* eye-like phenotypes (Figure S3, A–D). To verify the causal relationship between the *L* eye phenotype and ectopic expression of *L-RB*,

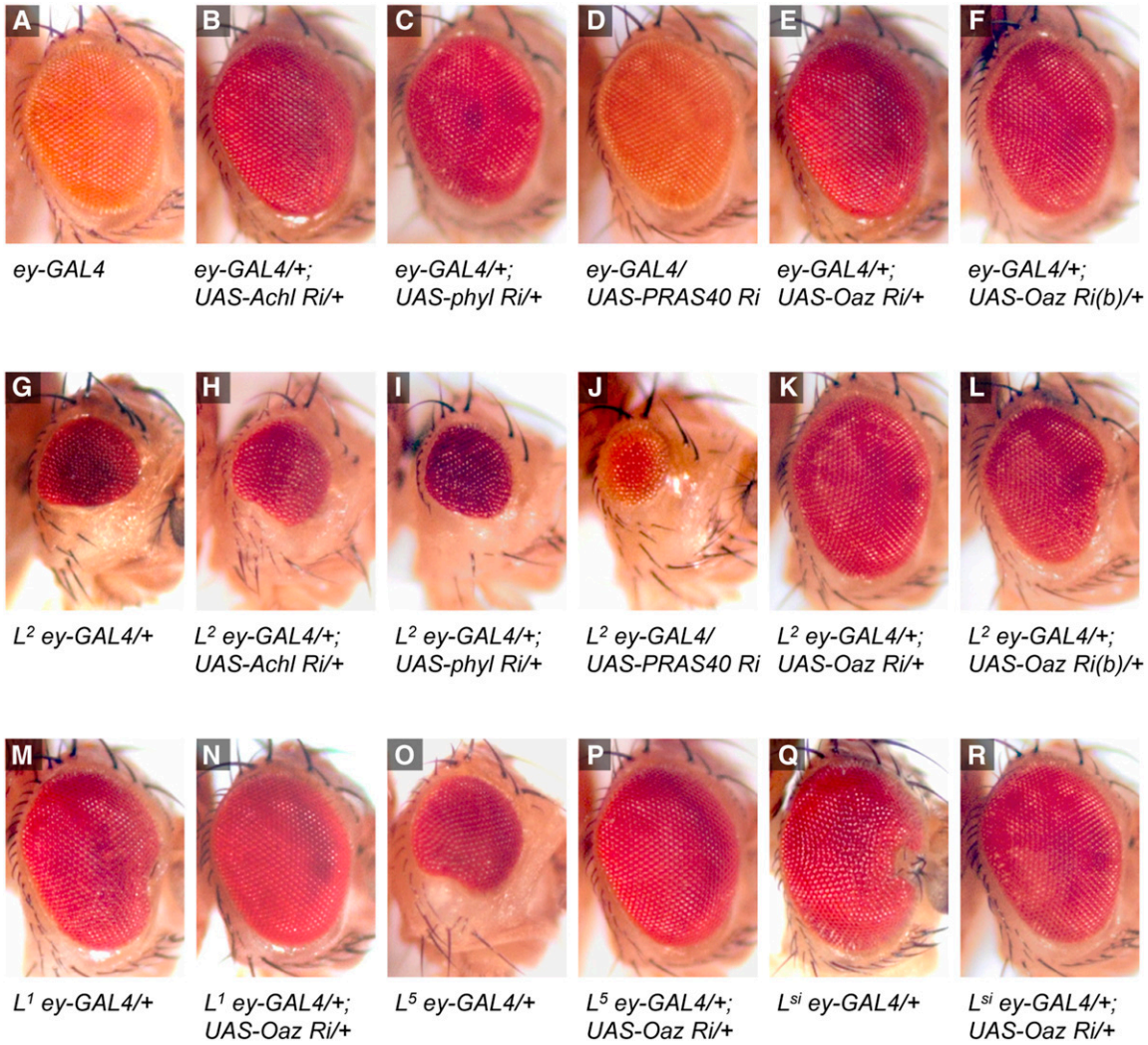

Figure 2 Suppression of dominant *L* eyes by *Oaz* knockdown. (A–L) Suppression of L^2/+ eye phenotype by reducing *Oaz* levels by *ey-GAL4*. Control knockdown by *Achl* RNAi (*Ri* in short) (B), *phyl* RNAi (C), *PRAS40* RNAi (D), and *Oaz* RNAi (E and F) did not affect eye development. (G) Control L^2 *ey-GAL4*/+ shows a typical L^2/+ eye phenotype. *Achl* RNAi (H), *phyl* RNAi (I), and *PRAS40* RNAi (J) failed to modify the L^2/+ phenotype. In contrast, two independent *Oaz* RNAi lines suppressed the L^2/+ phenotype completely (K) or strongly (L). (M–R) Suppression of other *L* dominant alleles by *Oaz* RNAi. Heterozygous L^1 and L^{si} show mild eye phenotypes like anterior dents (M and Q, respectively). L^5/+ eyes are affected more strongly (O). These dominant eye phenotypes of L^1, L^5, and L^{si} were fully suppressed to the wild-type level by *Oaz* RNAi (N, P, and R, respectively). All eye images were taken from female flies using the ZEISS Axiocam Microscope system. Sex chromosomal genotypes are $y^1\ v^1/\ w^{1118}$ or $y^1\ sc^*\ v^1/\ w^{1118}$, except (A, D, and J) that have w^{1118}, in which *L* phenotypes tend to be weakly enhanced. *Achl Ri* (B and H) is *P[TRiP.JF01976]*. *phyl Ri* (C and I) is *P[TRiP.JF03369]*. Refer to Materials and Methods for *PRAS40 Ri* (D and J). *Oaz Ri* (E, K, N, P, and R) is *P[TRiP.GLV21080]*. *Oaz Ri(b)* (F and L) is *P[TRiP.JF01943]*. Variations of *L* eye phenotypes were minimized by backcrosses. Penetrance of the *L* dominant eye phenotypes was: >90% for L^2/+ (G), >70% for L^1/+ (M), 50–70% for L^5/+ (O), and 60–80% for L^{si}/+ (Q). For each genotype, >1000 flies were examined in different batches. Suppression of *L* eye phenotypes by *Oaz* RNAi (K, N, P, and R) was nearly 100% ($n > 500$).

we targeted *L-RB*-specific sequences of the *L-RB* exon 1 (Figure 5A) using the CRISPR-Cas9 method in *L* dominant alleles.

Transgenic flies expressing the specific gRNA sequences were crossed with L^2 or L^5 allele expressing Cas9 under the ubiquitous *Act5C* promoter (*Act-Cas9*). This somatic CRISPR targeting induced a wide range of suppression of the L^2/+ eye phenotype due to different levels of *L-RB* mutant cells in the mosaic eyes (Figure S6, L^2/+, *Act-Cas9* > *U6-cbm1*). These data from the somatic targeting indicate that the L^2/+ eye phenotype is dependent on the level of *L-RB* function. However, L^5/+ eyes were scarcely affected in the same somatic CRISPR targeting. Because L^5/+ eyes were restored successfully by RNAi targeted to common sequences shared by both *L* splice forms (Figure 2P), the lack of *L-RB* targeting effects on L^5/+ supports that the L^5 dominant phenotype is largely dependent on the *L-RC* form rather than *L-RB*, which is consistent with the *hopper[ ]*L^5 insertion near the first exon of *L-RC*.

We also generated germline mutations in *L-RB* as suppressors of L^2 from a genetic screening of the *L-RB*-specific CRISPR targeting (Figure 5, I and J). L^{b5} showed a 29-bp deletion comprising the 3′-end of *L-RB* exon 1 and the 5′-splicing donor sequence of intron 1. As for L^{b6}, a sequence

A

```
MMALKMLYRGPSSRLENLIEKIQATKEITNNDMYSTHTSSSYSPSISDGTMTPNSHHLIGAPTAAGQEDHPTEGKINGGADGEDLPKPKR   90   REF

LPHFHHHHHHHYHHQQALKIANKLRKINKEAKMGATAGGGATGAASKFDKLTGEGIKSRGDGSYQCQFCEKTFPRLGYLKHHVQSHAEHL  180   REF
LPHFHHHHHHHYHHQQALKIANKLRKINKEAKMGATAGGGATGAATKFDKLTGEGIKSRGDGSYQCQFCEKTFPRLGYLKHHVQSHAEHL        Mohr

PFKCEYCSKLFKHKRSRDRHKKLHTNERNYKCPHCEAAFSRSDHLKIHMKTHDIQKPFQCSMCNRGYNTAAALTSHMQKHKKNAAILAAG  270   REF

GNPNALNYSPRSTGSASASVSSNGSLQKRRYALALASDSSPSRMDFPKRSRSNHVGGTTTTATPTPLLRCSYCPKVTEFSSLEQLNAHLQ  360   REF
GNPNALNYSPRSTGSASASVSSNGSLQKRRYALALASDSSPSRLDFPKRSRSNHVGGTTTTATPTPLLRCSYCPKVTEFSSLEQLNAHLQ        Lsi, Lfee

SVHEQPQTQAVKTPVQEGEGFQLSCEYCTMKFGNIAGLFQHMRSTHMDRLSSPNSYYEHFNRLATAGTFSPRLALDLPKIKPDLGSPERE  450   REF
SVHEQPQTQGVKTPVQEGEGFQLSCEYCTMKFGNIAGLFQHMRSTHMDRLSSPNSYYEHFNRLATAGTFSPRLALDLPKIKPDLGSPERE        w1118, Mohr, L4

                                                ZF7                                          ZF8
SRPAEDDLPTDLSNNKRRPLTPNPQAQTPLAPPSAPPGVFFCNQCNAGLPDFESFRNHLKSHIAEGMQLVCPHCGMSLPEQSEFERHVVG  540   REF

          ZF9                                   ZF10                                   ZF11
HFLITGSEFNCSSSCGKSFAKSEDLQQHLLSEHVLTLLKCSLCSELCESRMAMQLHLACAHSQETKLLRCSACLELFRSDAEFHVHVKTR  630   REF
HFLITGSEFNCSSSCGKSFAKSEDLQQHLLSEHVLTLLKCSLCSELCESRMA------CAHSQETKLLRCSACLELFRSDAEFHVHVKTR        Lrev6-3

                ZF12                                  ZF13
HQLGGHPTLGATSSAPTNPLQCMFCRAVCSSELEMHFHLAAHARQFRCPSCPETFHVEFLLDRHMQSQHGGVKDKEANSPNMGSLYVNAL  720   REF

LPPLAAAAAAAAATNNNSSIIDYNVAFKGLFGGASGGAGSGGGGAQSGGAPPSANKFYSPLQVDTNALKAQTSPHPALMYGLSQRYLMEM  810   REF

YAAKSTSPSGNEGVGNSQPPAPQATAPPPPPNASTATFSCGMCERQDLRSEAELHSHRKLAHNLKTGVSLRCAYCAGNFKSRAELEQHMK  900   REF

SCHNSTGKHKCLICDEVFPSPAILAEHKLQHSKVGQSGKCSHCGQPLEDVAAFRAHLSEHGSDGASLPLACICCRQTLHSEFELSLHAKF  990   REF

HTKSSSSGGSLQEPVCALCLEPLPDATEGPAKLCDKCCRKHNLNGKRGKHSEPATSLPAPPSAFVENRCNLCKMILPHAQKLQEHLVEHT 1080   REF
HTKSSSSGGSLQEPVCALCLEPLPDATESPAKLCDKCCRKHNLNGKRGKHSEPATSLPAPPSAFVENRCNLCKMILPHAQKLQEHLVEHT        w1118

FAGTEQRGFNCYICSAVFTAPGGLLNHMGEHGAHSRPYDCNLCPEKFFFRAELEHHQRGHELRPQARPPAAKVEVPSIRNTSPGQSPVRS 1170   REF
FAGTEQRGFNCYICSAVFTAPGGLLNHMGEHGAHSRPYDCNLCPEKFFFRAELEHHQRGHELRPQARPPAAKVEVPSIRNTSPGQSPLRS        w1118, L4, Lsi

PTIVKQELYETDTVESAGVEDEPENHPDEEEYIEVEQMPHETRPSGIGSQLERSTSSA 1228                                    REF
PTIVKQELYETDTVESAGVEDEPENHPDEEEYIEVEQMPHETRPSEIGSQLERSTSSA                                          w1118, Mohr, L4, Lsi
PTIVKQELYETDTVESAGVEDEPENHQDEEEYIEVEQMPHETRPSGIGSQLERSTSSA                                          Lfee
```

B

Amino acid polymorphisms in L/Oaz-PB	w^{1118}	*Mohr* strains ft^1, L^1, L^2, L^5, L^r	$L^{rev6\text{-}3}$	L^4	L^{si}	L^{fee}
S136T		O	O			
M314L					O	O
A370G	O	O	O	O		
G1019S	O					
V1168L	O			O	O	
P1197Q						O
G1216E	O	O	O	O	O	
ΔMQLHLA of the 10th ZF			O			

Figure 3 Identification of $L^{rev6\text{-}3}$ mutation and polymorphisms in *L* mutants. (A) Localization of the $L^{rev6\text{-}3}$ deletion in *Oaz* coding sequence. Oaz peptide sequences (coding product of *Oaz-RB*) of control stocks and *L* mutants were deduced from genomic sequencing results. Blue letters represent the multiple ZF motifs found in Oaz sequences. Compared to the FlyBase reference sequences (REF in gray), all the examined stocks including w^{1118} showed specific polymorphisms (red letters) in peptide sequences as well as numerous nucleotide polymorphisms. $L^{rev6\text{-}3}$ has a small deletion of six amino-acids in the 10th ZF motif (blue box), but not in L^2 or other *Mohr* strains (ft^1, L^1, L^2, L^5, and L^r). This deletion is located within the putative Mad-binding motif (ZF7 to ZF13 in bold blue). (B) Summary of amino-acid polymorphisms identified in deduced Oaz sequences of examined stocks of the control w^{1118}, ft^1, and *L* mutants, as compared to the FlyBase reference. Polymorphic amino acid changes are indicated as red characters in (A).

substitution in the CRISPR target site resulted in a frame-shift from the 24th codon of L-PB followed by early translation stop (Figure 5N). Both L^{b5} and L^{b6} mutations suppressed the $L^2/+$ eye phenotype, resulting in a partial rescue like the hypomorphic $L^{rev6\text{-}3}$ allele (Figure 5, E, I, and J). L^{b5} and L^{b6} could not complement all *L* loss-of-function mutations tested including $L^{rev6\text{-}3}$ and L^{D0B}, indicating that the *L-RB* splice form is necessary for normal development.

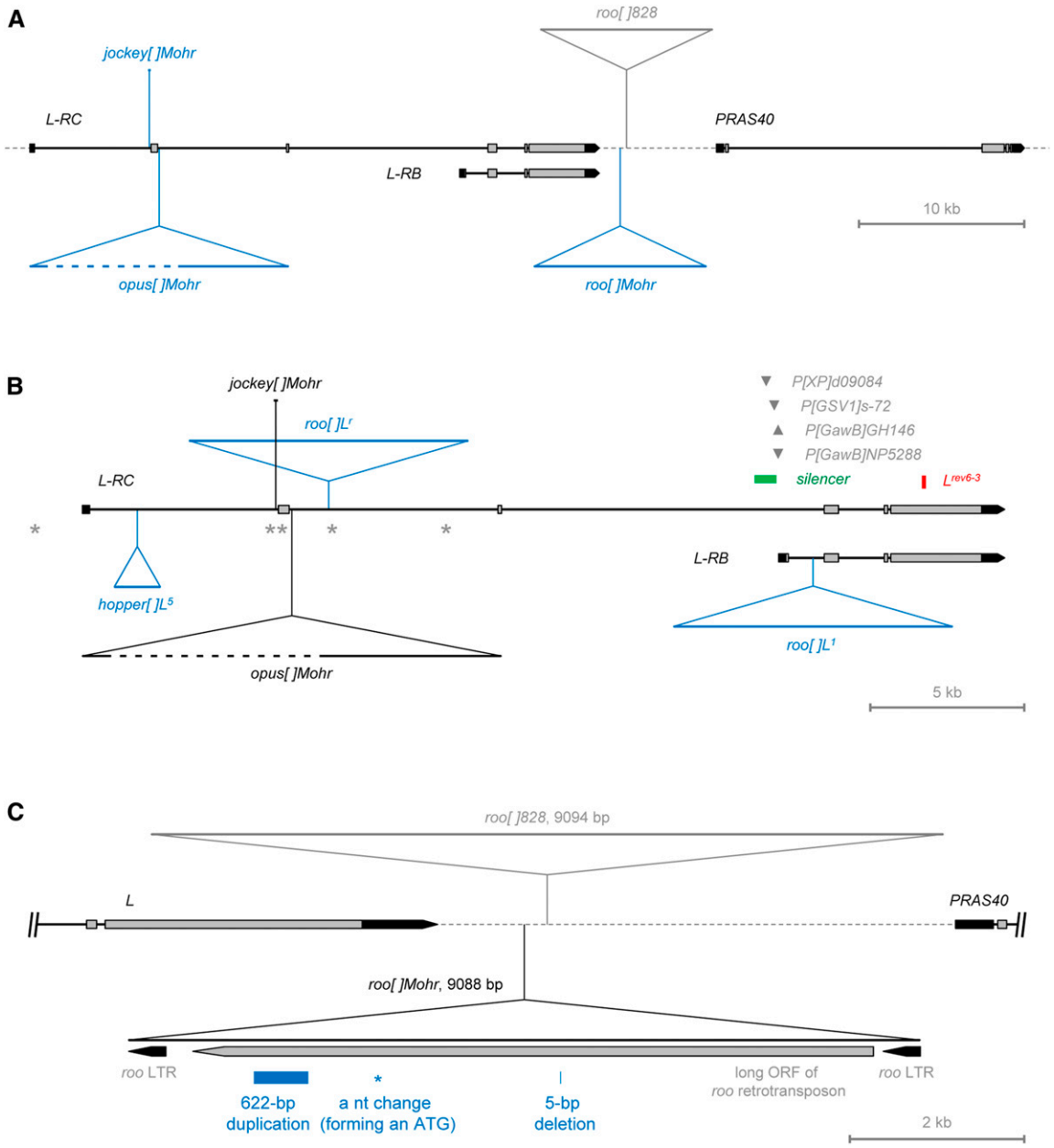

Figure 4 Molecular mapping of *L* mutations. (A) Identification of natural transposons shared by *Mohr* strains (*ft*^{1}, *L*^{1}, *L*^{2}, *L*^{5}, and *L*^{r}). A genomic map of *L*/*Oaz* is adapted from the FlyBase Genome Browser. Shared transposon insertions were found in or nearby the *L* region: *opus[ ]Mohr*, *roo[ ]Mohr*, and a remnant sequence of *jockey[ ]Mohr* (blue triangles). The dotted line inside *opus[ ]Mohr* indicates an undefined part of the transposon that could not be amplified by PCR. Note that *roo[ ]Mohr* is different from *roo[ ]828* (gray triangle) described in the FlyBase reference genome. (B) Allele-specific transposons were found in dominant *L* mutants: *roo[ ]L*^{1}, *roo[ ]L*^{r}, and *hopper[ ]L*^{5} (blue triangles). A silencer *cis*-element, which is the putative target sequence for Polycomb-silencing (Negre *et al.* 2011), is indicated as a green box. Possible insulator elements (Negre *et al.* 2010) are indicated as asterisks. Gray triangles indicate P-element insertions in upstream sequences of *L-RB*, and a red bar indicates the small deletion in *L*$^{rev6\text{-}3}$. (C) Identification of *L*^{2}-specific alterations found within the transposon sequence of *roo[ ]Mohr*. A 622 bp duplication, a 5 bp deletion, and a nucleotide change are indicated by blue colors.

CRISPR mutagenesis in the L region involves homology-directed repair of targeted DNA breaks

We have sequenced the entire *L* region except for the *opus[ ]Mohr* transposon inserted near the *L-RC* exon 2. As described above, *opus[ ]Mohr* is shared by *Mohr* strains including classical *L* dominant alleles and the control *ft*^{1} (Figure 4A). Therefore, although we found alterations in the 3′ intergenic *roo[ ]Mohr* of *L*^{2} mutant, it was necessary to test whether *opus[ ]Mohr* in *L*^{2} mutant has no change from that of the *ft*^{1} control strain. However, we could determine only ~6 kb terminal regions from both ends of *opus[ ]Mohr* probably because more interior part of the transposon could not be amplified by PCR, perhaps due to a structural change in *opus[ ]Mohr* such as insertion of extraneous repetitive sequences.

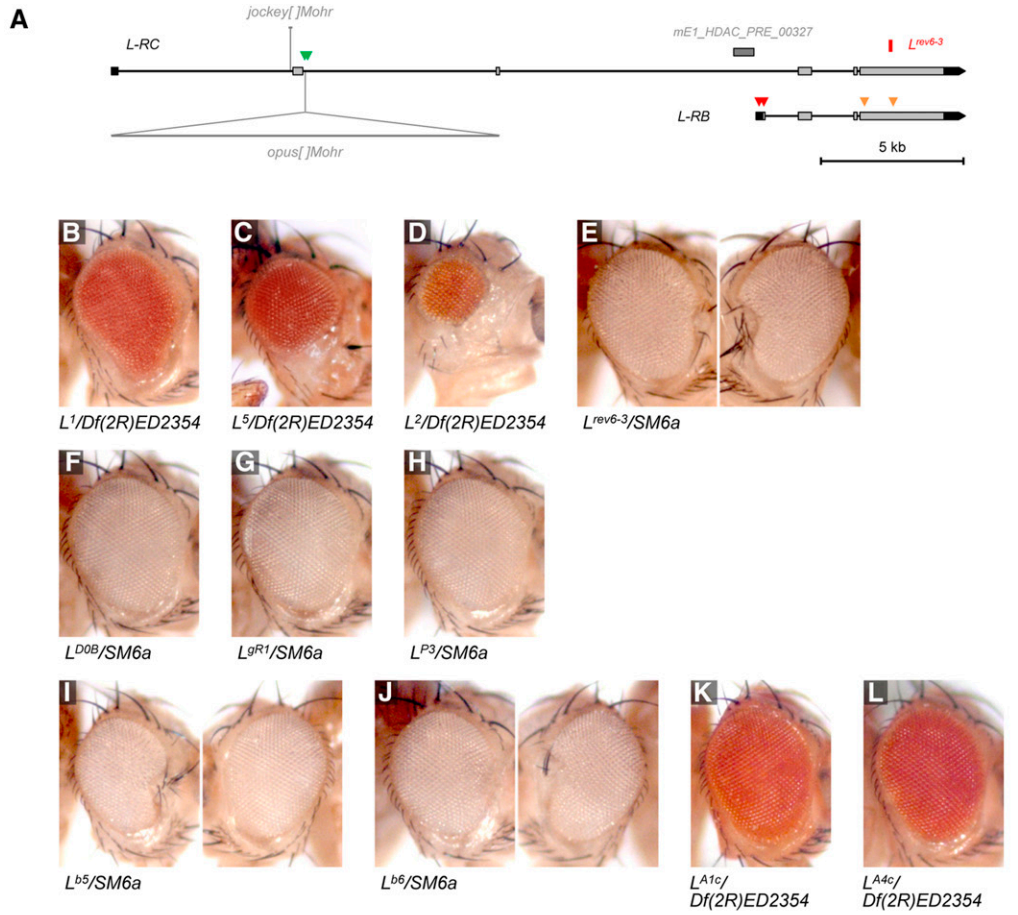

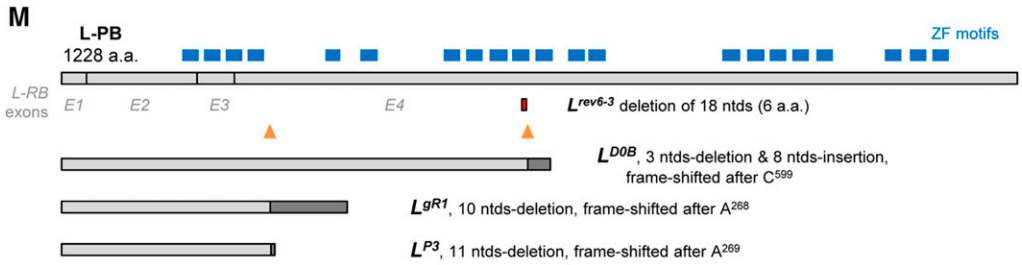

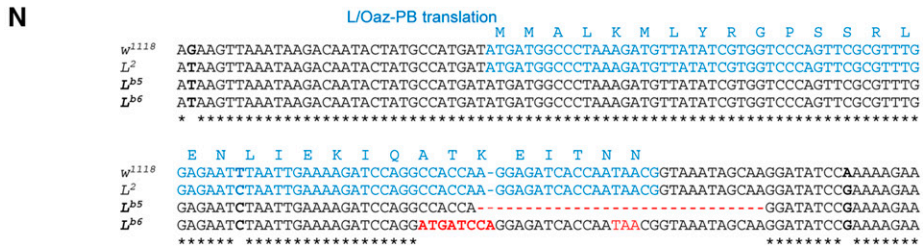

Figure 5 Reversion of dominant *L* eye phenotypes by loss-of-function mutations of *L*. (A) CRISPR genomic target sites for *opus[ ]Mohr*, *L-RB* exon1, and *L* coding sequence are indicated by green, red, and orange arrowheads, respectively. (B–D) Heterozygous eye phenotypes of classical *L* mutations of *Mohr* strains, L^1 (B), L^5 (C), and L^2 (D). These *L* mutants are viable in transheterozytes with *L*-uncovering deficiencies such as *Df(2R)ED2354* that carries a *mini-white* (w^{+m}) transgene at the proximal breakpoint of the deficiency. (E) A L^2-reversion mutant, $L^{rev6\text{-}3}$, cannot complement *L*-uncovering deficiencies, resulting in lethality. The mutant heterozygotes show normal or mild eye reduction. Both left and right eyes of an individual are presented to show phenotypic variation. (F–H) New L^2 eye-reversion alleles, L^{D0B} (F), L^{gR1} (G), and L^{P3} (H), could not complement the lethality of $L^{rev6\text{-}3}$ and *L*-uncovering deficiencies, suggesting that all these mutations are allelic to *L*. Heterozygotes of these alleles show normal eyes. (I and J) *L-RB*-specific lethal mutations. Left and right eyes from an individual show variable phenotypes in L^{b5}/*SM6a* (I) and L^{b6}/*SM6a* (J). (K and L) L^2-revertants from *opus[ ]Mohr* targeting. All reversion lines including L^{A1b} (K) and L^{A4c} (L) are viable in transheterozygotes with *L*-uncovering deficiency *Df(2R)ED2354*. These lines lost the L^2-specific *roo[ ]Mohr* during the CRISPR mutagenesis (see text for details). (M) Deduced translations from lethal *L* mutations (L^{D0B}, L^{gR1}, and L^{P3}) in coding sequences of the last exon. Blue boxes indicate the ZF motifs found in the *Drosophila* Zfp423 family protein, and orange arrowheads indicate the CRISPR target sites. The location of the $L^{rev6\text{-}3}$ deletion of six amino acids is also indicated. Dark gray boxes indicate aberrant coding sequences caused by the frame-shift mutations prior to stop codons. (N) Nucleotide sequence alignment of *L-RB*-specific L^2 eye-reverting mutations, as compared to the progenitor L^2 or the w^{1118} control sequences. The InDel mutations are indicated by red letters or a dashed line, respectively. Blue letters for the coding sequence of *L-RB* exon 1. Bold letters for polymorphic sequences. Frequencies of the *L* dominant eye phenotypes shown in the (B−L). are: 60–80% for L^1/*SM6a* (B), 40–60% for L^5/*SM6a* (C), >90% for L^2/*SM6a* (D), 40–80% for $L^{rev6\text{-}3}$/*SM6a* (E), >90% for L^{D0B}/*SM6a* (F), 100% for L^{gR1}/*SM6a* (G) and L^{P3}/*SM6a* (H), 40–80% for L^{b5}/*SM6a* (I) and L^{b6}/*SM6a* (J), and 100% for L^{A1c}/*SM6a* (K) and L^{A4c}/*SM6a* (L), respectively ($n >$ 1000 for each genotype).

As an alternative approach, we attempted to excise the *opus[ ]Mohr* transposon by CRISPR mutagenesis and see whether the L^2/+ eye phenotype can be reverted by removing the transposon. To excise *opus[ ]Mohr*, we used *U6-DE1* transgene expressing gRNA to target two sites flanking the insertion in the intron 2 of *L-RC*: one at 58 bp before

the proximal *opus* LTR and the other at 292 bp after the distal LTR of the transposon (target sites as green arrowheads in Figure 5A, see *Materials and Methods*). Somatic targeting of the *opus[ ]Mohr* with ubiquitous Cas9 expression showed variegated suppression of the $L^2/+$ phenotype as seen in the previous targeting of *L-RB* exon 1 (Figure S6, $L^2/+$, *Act-Cas9 > U6-DE1*). This suppression seemed to be specific to L^2 since $L^5/+$ eyes were rarely modified by the same somatic targeting.

We then isolated 22 independent L^2-revertant lines from the germline CRISPR mutagenesis. All of these lines showed complete reversion of the $L^2/+$ eye phenotype (Figure 5, K and L). Intriguingly, these lines could also complement the lethality of *L* loss-of-function mutants, such as L^{D0B}, L^{gR1}, and *Df(2R)ED2354*, indicating that targeted removal of *opus[ ]Mohr* did not impair the function of *L*. These L^2-revertants were analyzed at the molecular level to determine whether the reversion was due to loss of *opus[ ]Mohr*. In about half of the revertants (12 of 22 lines), the *opus[ ]Mohr* transposon was either completely excised or mostly deleted except an *opus* LTR at the end. Conversely, the other half of reversion lines (10 of 22 lines) showed no difference from the original L^2 sequence or only minor changes in sequenced amplifiable regions of the transposon. Hence, the insertion of *opus[ ]Mohr* transposon may not be responsible for the $L^2/+$ eye phenotype, raising a possibility that reversion of the $L^2/+$ eye phenotype might be due to a different change in the *L* region during *opus[ ]Mohr* targeting.

In an attempt to identify such change, we further analyzed *L* region in L^2-revertant lines by using genomic polymorphisms between L^2 and the other homologous chromosome. Remarkably, analysis of polymorphic markers in L^2-revertant lines revealed frequent recombination between L^2 and L^+ homologous chromosomes around target sites. In all 22 reversion lines, the 5′ intergenic region consists of the L^2 chromosomal sequences whereas the 3′ intergenic region was derived from the homologous *Sco*-marked L^+ chromosome. This indicates that two parental chromosomes were recombined around the CRISPR target sites during the mutagenesis, which resulted in the loss of the L^2-specific *roo[ ]Mohr*. Since the loss of *roo[ ]Mohr* in the 3′ intergenic region coincides with complete loss of $L^2/+$ phenotype, the L^2-specific alteration in the *roo[ ]Mohr* transposon appears to be a major cause of the $L^2/+$ eye phenotype.

Our data above suggest that CRISPR mutagenesis is accompanied by homology-dependent repair (HR) of the targeted DNA break and/or homologous recombination in the male germline expressing Cas9. We further tested the HR-dependency of CRISPR targeting events by using deficiency chromosomes that cover or uncover the targeted *L* region. Chromosomal deficiencies that uncover *L* (*Df(2R)ED2354*, *Df(2R)BSC357*, and *Df(2R)BSC668*, Figure 1A) and cover the targeted region (*Df(2R)BSC700* and *Df(2R)Exel8059*, Figure 1A) were made transheterozygous with L^2 in the presence of *vas-Cas9 > U6-DE1* or *vas-Cas9 > U6-cbm1* (mutagenic F1 males genotype: *vas-Cas9/Y*; L^2*/Df(2R)X*; *U6-L-gRNA/TM2*). As expected, no L^2-revertant F2 progeny was found from CRISPR targeting when L^2 was transheterozygous with deficiencies that uncover *L*. In contrast, dozens of L^2-revertants were collected when L^2 was heterozygous with deficiencies that cover *L* (Table S2). Further, we could also detect frequent phenotypic recombinations between L^2 eye and *mini-white* (w^{+m}) eye color marker associated with *Df(2R)BSC700* (proximal to *L*). Next, we tested another homologous chromosome, $PRAS40^{EY10689}$, which also possesses CRISPR target sites in the *L* region. From the mutagenic transheterozygotes ($L^2/PRAS40^{EY10689}$), we could collect L^2-revertants. However, no phenotypic recombinant of L^2 and w^{+m} eye was found because both the L^2-specific *roo[ ]Mohr* and the *PRAS40* *P*-element w^{+m} marker are located distal to the CRISPR target sites. This suggests that the CRISPR target sites had been recombination breakpoints between the distal L^2 and the proximal w^{+m} of *Df(2R)BSC700* (Table S2).

Altogether, these results suggest that L^2 suppression by CRISPR targeting at *opus[ ]Mohr* was due to loss of the L^2-specific *roo[ ]Mohr* through the HR pathway or meiotic recombination between L^2 and its homologous chromosome in mutagenic F1 males.

L protein is expressed ectopically in $L^2/+$ eye disc

Our data so far suggest that *L* dominant eye phenotypes are likely due to abnormal regulation of *L* in eye discs. To identify the misexpression of L protein, we generated anti-L antiserum by using a 461 aa C-terminal L protein fragment containing eight Zn-finger motifs. In wild-type, anti-L immunostaining was not detected in eye disc (Figure 6A and Figure S3G), although there was a strong expression in other tissues including embryonic and larval brain, ventral ganglion, anterior and posterior spiracles, and leg disc (Figure S7). In addition to the reported *L* function in the posterior spiracle development (Krattinger *et al.* 2007), we found that *L* RNAi or mutation causes loss of adult claws (Figure S7, E–G), indicating that L expression in the distal region of leg disc (Figure S7D) is important for claw development. We also examined the pattern of *L* transcription by using *L-GAL4* insertion lines (*P[GawB]NP5288* and *P[GawB]GH146*, Figure 4B) as reporters. In wild-type, *L-GAL4* expression was also undetectable in eye disc (Figure 6D), whereas it was strongly expressed in posterior spiracles and larval/adult brains (Figure S7C and Figure S9).

Next, we examined whether L protein is expressed ectopically in $L^2/+$ or $L^{rev6\text{-}3}/+$ mutant eye discs. Since the reduction of eye discs can be clearly detected already in the second instar larvae, we examined $L^2/+$ eye discs from the larval stage. Anti-L staining was not detected in early second instar discs. However, we found ectopic L expression in $L^2/+$ eye discs from the late second- to early third-instar larvae (Figure 6B). Ectopic L expression was enriched mainly along the dorsoventral (DV) midline of the late second-instar eye disc. In early third-instar eye discs where retinal differentiation has been initiated, ectopic L expression was detected along the

DV boundary in the undifferentiated anterior region (Figure 6B). However, this expression pattern was not maintained in later third-instar stages, probably due to the preferential loss of ventral tissues (Singh *et al.* 2006).

We also examined eye discs from $L^{rev6\text{-}3}/+$ larvae. Since $L^{rev6\text{-}3}$ is an inframe small deletion (6 aa) mutation that partially suppresses the $L^2/+$ eye phenotype (Figure 3A), we reasoned that the mutant may express the mutated L protein in nearly normal shaped eye discs. Indeed, we could confirm the DV midline pattern of ectopic L expression in normal shaped $L^{rev6\text{-}3}/+$ eye discs (Figure 6C), although the expression level was weaker than that of $L^2/+$ eye discs.

L-GAL4s are expressed ectopically in eye disc by the L^2-specific roo transposon

The observation of ectopic L protein in $L^2/+$ eye discs suggests that L^2 mutation may cause the misregulation of *L* gene expression. To test whether L^2 mutation leads to transcriptional misregulation of *L*, we used intrinsic reporter activities of *L-GAL4* insertions (*P[GawB]GH146* and *P[GawB]NP5288*). The expression of these *L-GAL4* reporters was not affected by *L* mutations in *trans* position. Therefore, we decided to generate recombinants between *L-GAL4* insertions and L^2-specific *roo[ ]Mohr* transposon and test whether *L-GAL4* activity can be induced ectopically by L^2 in *cis* position. Since *L-GAL4* and *roo[ ]Mohr* are <9 kb apart, it would be difficult to generate recombinants by conventional meiotic recombination. Hence, we utilized our finding that the HR-dependent CRISPR targeting in the germline can trigger male recombination around the target site. We designed a CRISPR mutagenesis to induce recombination between *L-GAL4* insertions and L^2–specific *roo[ ]Mohr*. CRISPR target sequences were chosen in the regions proximal or distal to *L-GAL4* insertions. Proximal and distal guide RNA was encoded by *U6-csm1* or *U6-cbm1* gRNA construct, respectively, as shown by red arrowheads in Figure S8A. Targeting was induced in F1 males of L^2/*L-GAL4*, *vas-Cas9* > *U6-cbm1* (or *U6-csm1*). Interestingly, only the distal targeting by *cbm1* transgene could generate *L-GAL4* L^2 recombinants that show red eye color with L^2 eye phenotypes (either parental L^2-like or partially suppressed). Sequence analysis of these recombinant lines confirmed the presence of both *L-GAL4* and *roo[ ]Mohr*. Among those, recombinants showing strong L^2 suppression had frame-shifting deletions in the targeted *L-RB* exon 1. Conversely, other recombinants showing weak or no suppression had inframe changes in the *L* gene (Figure S8A), consistent with the data that L^2 phenotype is suppressed by reduced *L* function (Figure 2, Figure 3, and Figure 5).

To detect ectopic *L-GAL4* expression in these *cis*-recombinants carrying the GAL4 driver and L^2 mutation, we examined GAL4 activities in eye discs by using the G-TRACE system (Evans *et al.* 2009) that allows both real-time expression and clonal expression of *L-GAL4*. Unexpectedly, upon crossing with the G-TRACE reporter, the heterozygous L^2-recombinants (*L-GAL4* L^{2*}/*UAS-RFP*, *UAS-FLP*, *Ubi>>GFP*) showed abnormally delayed larval growth, resulting in few adult survivors for an unknown reason. In contrast, no developmental defect was noticed in the progeny from control crosses between the G-TRACE reporter and the original *L-GAL4* insertions or L^2. Normally, *L-GAL4* expression is prominent in larval posterior spiracles and larval/adult brains (Figure S9). In these tissues, the real-time (*L-GAL4* > *RFP*) and clonal reporter expression (*L-GAL4* > *FLP*, *Ubi>>GFP*) in *L-GAL4* L^2 recombinants were indistinguishable from the control *L-GAL4* reporter expression pattern of nonrecombinants. Reporter expression patterns were similar in different recombinant lines showing L^2 suppression.

As expected, neither real-time nor clonal reporter expression was detected in wild-type eye discs carrying the control *L-GAL4* insertions (*P[GawB]GH146* or *P[GawB]NP5288*) (Figure 6D). However, we detected ectopic GAL4 activity in eye discs from *L-GAL4* L^2 recombinants (Figure 6, E and F). The real-time *L-GAL4* activity (*L-GAL4* > *RFP*) was enriched along the DV boundary region of eye disc similar to the pattern of ectopic L protein expression in $L^2/+$ and $L^{rev6\text{-}3}/+$ mutant eye discs (Figure 6, B and C). However, the clonal reporter expression (*L-GAL4* > *FLP*, *Ubi>>GFP*) was much broader to cover most part of the eye-antennal disc, suggesting that L is expressed more broadly in $L^2/+$ eye discs at early stages. Such ectopic reporter expression was consistently found in different L^2-recombinants like L^{GDb1} (*P[GawB]GH146* recombined with L^2) or L^{5Db5} (*P[GawB]NP5288* recombined with L^2), suggesting that ectopic expression is induced by the L^2 mutation. Despite the ectopic *L* reporter expression, these eye discs showed nearly normal eye shape since functional L-PB protein is not expressed due to the frameshift mutations in L^{GDb1} and L^{5Db5}.

Taken together, these data suggest that L^2 dominant eye phenotype is due to misexpression of *L* in eye disc induced by the altered form of *roo[ ]Mohr*.

Discussion

We have presented genetic and molecular evidence that *Oaz* is the *L* gene. Our data show that *L* dominant eye phenotypes can be restored by reducing the level of *L* and that L expression is ectopically induced in $L^2/+$ mutant eye disc. These results suggest that classical *L* dominant alleles are gain-of-function mutations that inhibit eye development by causing *L* misexpression.

Role of transposable elements in L dominant phenotypes

Our data reveal that all classical *L* dominant mutants tested are gain-of-function mutants associated with the insertion of natural transposons in the *L* region. All *Mohr* strains including the control ft^1 share two retrotransposons, *opus[ ]Mohr* near *L-RC* exon 2 and *roo[ ]Mohr* in the 3′ intergenic region of *L*, as well as a fragment of *jockey* element (Figure 4). In addition to these common insertions, each of *L* dominant mutants carry an additional specific transposon such as *hopper[ ]*L^5, *roo[ ]*L^1, or *roo[ ]*L^r, which were not found in the ft^1 control strain. These allele-specific transposons were inserted in different introns of the *L* transcription unit.

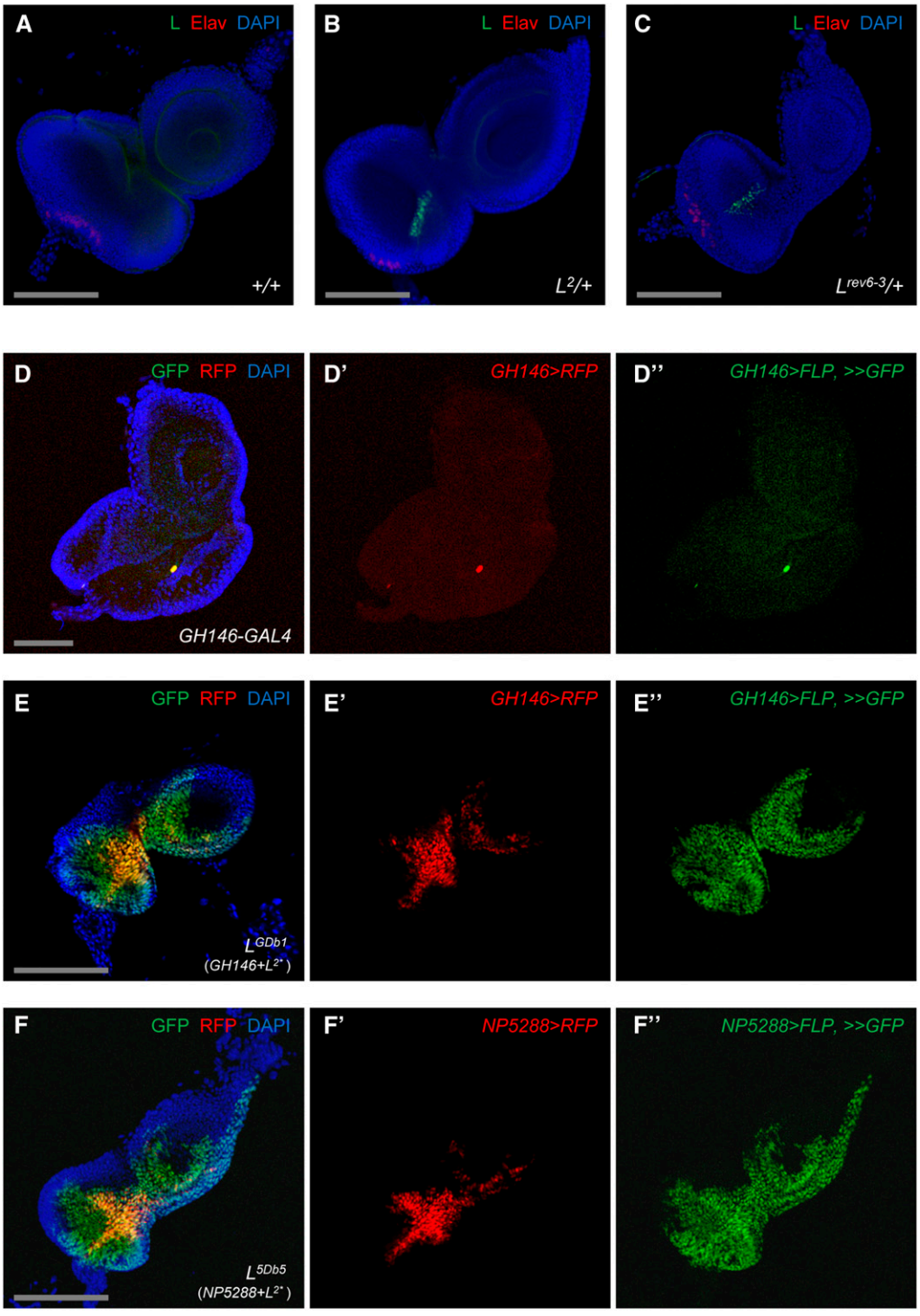

Figure 6 Ectopic *L* expression in *L* mutant eye discs. (A–C) Anti-L antiserum staining in early third instar larval eye discs. No L immunostaining was detectable in eye-antenna imaginal discs of control stocks (A). Ectopic L expression was detected in L^2/+ mutant eye discs (B) and $L^{rev6\text{-}3}$/+ eye discs (C) from the late second to early third instar larvae. (D–F) Ectopic GAL4 activities in L^2/+ mutant eye discs. *L-GAL4* L^2 recombinants were used to detect ectopic *L-GAL4* (*P[GawB]GH146* or *P[GawB]NP5288*) activities in third instar eye discs. Real-time *L-GAL4* expression and clonal expression were visualized by RFP and GFP, respectively, using the G-TRACE system. Control *L-GAL4* without recombination with L^2 showed no GAL4 expression in eye discs (D–D″). Ectopic GAL4 expression was clearly detected in L^{GDb1} (*P[GawB]GH146* + L^2) recombinant discs (E–E″) and L^{5Db5} (*P[GawB]NP5288* + L^2) recombinant disc (F–F″). Two *L-GAL4*s, *P[GawB]GH146* and *P[GawB]NP5288*, show similar ectopic GAL4 activities. Bar, 100 μm. Full genotypes for (D–F) are as follows: (D) y^1 *w*/ w*; P[GawB] GH146/ P[UAS-RFP], P[UAS-FLP], P[UAS>>GFP]*, (E) y^1 *w*/ w*;* L^{GDb1}*/ P[UAS-RFP], P[UAS-FLP], P[UAS>>GFP]*, and (F) y^1 *w*/ w*;* L^{5Db5}*/ P[UAS-RFP], P[UAS-FLP], P[UAS>>GFP]*.

Besides, we could also identify the L^2-specific mutations within the retroviral sequence of *roo[ ]Mohr*, although this transposon is shared by all *Mohr* strains. The L^2 mutation found in the 3′ intergenic region of *L* could induce ectopic GAL4 expression in eye disc when the *L-GAL4* insertions were in *cis* position with the mutation.

Among natural transposons found in the *L* region, *hopper* is a member of the terminal inverted repeats (TIR)-dependent DNA transposon family, and *opus* and *roo* elements are LTR family retrotransposons. These natural transposons are frequently found in different *Drosophila* strains (Kaminker *et al.* 2002; Kapitonov and Jurka 2003; Linheiro and Bergman 2012), and there have been several reports of spontaneous mutations associated with transposon invasions. The sex-lethal allele Sxl^{M4} is the only known mutation caused by *hopper* insertion (Bernstein *et al.* 1995). Hence, L^5 seems to

be the second example of *hopper*-induced mutation. Multiple *opus* insertions have been associated with developmental mutations such as *opus[ ]N$^{fa\text{-}1}$*, *opus[ ]lz^{34}*, and several *tube* mutations (Gorman and Girton 1992; Crew *et al.* 1997; Clemmons and Wasserman 2013), all of which are loss-of-function mutations. Dozens of *roo* retrotransposon-induced mutations have been reported, including a gain-of-function mutation, *Gla* (Brunner *et al.* 1999).

At least three possible mechanisms can be considered for how the insertion of the natural transposons in the *L* region can cause *L* dominant eye phenotypes. First, *L* might be misexpressed by regulators of the inserted transposons, as seen in *Gla* mutation. The *Gla* eye phenotype was proposed to result from *wg* misexpression in pupal eyes, driven by the *roo* LTR sequence inserted in the *wg* promoter region (Brunner *et al.* 1999). Similarly, a *Drop* mutation (*Dr^{Mio}*) with a *roo* family-related retrotransposon inhibits eye development by ectopic expression of the *Dr* gene that encodes an Msh homeobox transcription factor (Mozer 2001). *Gla* and *Dr^{Mio}* mutations by *roo* or *roo*-related retrotransposons affect late larval or pupal stage eye development. On the other hand, *L* mutant phenotypes can be detected in earlier larval stages prior to retinal differentiation.

Second, *L* mutant eyes may result from derepression of *L* silencing by transposon invasions. It is intriguing that putative Polycomb (Pc)-response element and tandemly aligned insulator elements have been identified in the *L* region (Nègre *et al.* 2010, 2011; Roy *et al.* 2010). Genome-wide analyses also indicated that the *L* region is highly enriched with chromatin domains for the Pc-mediated repression (Schwartz *et al.* 2006; Filion *et al.* 2010; Kharchenko *et al.* 2011). Interestingly, transposons associated with *L* dominant phenotypes are located near the insulator motifs or the Pc silencer (Figure 4B). Hence, *L* dominant eye phenotypes might be caused by altered epigenetic silencing of *L* expression by transposon insertions or by alterations within the existing retroviral element.

Third, *L^5* mutant has an insertion of *hopper[ ]L^5* near the first exon of the *L-RC* isoform, far from the insulator cluster (Figure 3B). *L-RB* form-specific CRISPR targeting strongly suppresses *L^2* mutation but has much weaker effects on *L^5*. In contrast, the *L^5*/+ phenotype is effectively suppressed by RNAi targeting both *L-RB* and *RC* forms. This suggests that the *L^5*/+ phenotype depends more on the *L-RC* splice form than the *RB* form. The N-terminal region of vertebrate Zfp423 family proteins contains a nuclear remodeling and histone deacetylation (NuRD) motif implicated in transcriptional repression of target genes including itself (Lin *et al.* 2004; Hong *et al.* 2005; Bond *et al.* 2008; Matsubara *et al.* 2009; Hesse *et al.* 2010). This motif is present in L-PC but not L-PB (Figure S4B). It remains to be studied whether the N-terminal motif of L-PC is also involved in transcriptional repression and whether *L-RC* is aberrantly transcribed by the *hopper[ ]L^5* insertion.

Homology-dependent repair of CRISPR targeting-induced DNA breaks

We used a variety of CRISPR targeting methods to characterize *L* dominant eye phenotypes. One of them was to revert the *L^2* dominant phenotype by targeted excision of the *opus[ ]Mohr*. In this process, we found that CRISPR targeting in the male germline results in frequent meiotic recombination at or around the target sites. Indeed, our data suggest that *L^2* suppression by the *opus[ ]Mohr* targeting was due to meiotic exchanges between *L^2* mutation and wild-type homologous chromosome rather than deletion of the transposon *per se*. However, when the same CRISPR targeting was made in *L^2* transheterozygous with chromosomes deficient in the *L* region, *L^2* suppression was not found, supporting its HR-dependency.

Compared to HR, the nonhomologous end-joining pathway (NHEJ) has been reported to be a fast and efficient DSB repair response, and mutagenesis by CRISPR targeting in *Drosophila* has been attributed largely to the error-prone NHEJ repair in the germline (Bier *et al.* 2018). However, the choice between competing DSB repair pathways is affected by multiple regulatory mechanisms depending on cell cycle or cellular contexts (Mao *et al.* 2008; Chapman *et al.* 2012; Zaboikin *et al.* 2017). For example, an analysis of several meiosis mutations revealed that NHEJ is negatively regulated in *Drosophila* oogenesis (Joyce *et al.* 2012). Our data also suggest that germline repair of induced DSBs during our CRISPR mutagenesis at *L* follows the HR pathway predominantly over NHEJ.

Using the targeted recombination strategy, we could successfully generate *L-GAL4 L^2* recombinants in *cis* position. These recombinant GAL4 reporters helped us demonstrate ectopic *L* expression by the *L^2* mutation in developing eye disc. Ectopic expression of *L-GAL4* reporter was also confirmed by the expression of L protein in *L^2*/+ mutant eye discs. These data suggest that the *L^2* eye phenotype is due to ectopic L expression in eye disc and provide an explanation for the suppression of all *L* dominant phenotypes by *L* RNAi or mutations.

Our results from G-TRACE experiments show that ectopic real-time expression of *L-GAL4* reporter is preferentially induced in the DV boundary region of the early third instar eye disc, while clonal *L-GAL4* expression is widespread in most part of the eye disc. Hence, *L-GAL4* seems to be expressed broadly in the early eye disc, but only the equatorial region remains to be active while dorsal and ventral expression is repressed by early third instar stage. As described above, all identified classical *L* mutations are associated with the insertion of natural transposons or alterations in the existing transposable element. It is possible that ectopic induction of *L* by transposable elements might antagonize critical genes involved in early eye development. The DV boundary pattern shows a similarity to that of *eyegone* (*eyg*)—a PAX-family gene important for early eye development (Jang *et al.* 2003; Dominguez *et al.* 2004; Yao and Sun 2005). Indeed, a reduced reporter expression of *eyg* was reported in a weak *L* dominant allele, *L^{fee}* (Wang and Huang 2009). Consistently, we had previously shown a phenotypic enhancement of another weak *L* eye, *L^{si}*, by reduction of *N* signaling (Chern and Choi 2002) that is required to maintain *eyg* expression in the growing eye primordium (Dominguez *et al.* 2004; Wang *et al.* 2008). It was also proposed that Eyg has the second function to repress *wg* expression that inhibits the initiation of retinal

differentiation in eye disc (Yao and Sun 2005; Ekas *et al.* 2006). It is noteworthy that the $L^2/+$ eye phenotype is suppressed by reducing Wg signaling (Singh *et al.* 2005, 2006). Molecular mechanisms for transposon-induced misregulation of *L* and affected regulators of eye development in different *L* mutants remain to be studied.

Identification of a molecular lesion for loss-of-function $L^{rev6\text{-}3}$ mutation

In the analysis of the $L^{rev6\text{-}3}$ mutation, we found a deletion of six amino acid residues in the 10th ZF motif located within the putative Mad-binding domain of L. Among the tandem repeats of ZF motifs, the central ZFs containing the putative Mad-binding domain is well conserved between the *Drosophila* L and its vertebrate homologs (Hata *et al.* 2000; Krattinger *et al.* 2007). Since the short deletion was uniquely found in $L^{rev6\text{-}3}$, this mutation is likely to be responsible for the intragenic suppression of the L^2 dominant eye phenotype. Because homozygous $L^{rev6\text{-}3}$ mutation is semi-lethal, the putative MAD-binding domain containing the 10th ZF motif seems to be critical for normal functions of L during development. The vertebrate Zfp423 family proteins interact with diverse transcription effectors, including SMAD proteins, O/E factors, retinoic acid receptors, the Notch intracellular domain, and HDACs (Tsai and Reed 1997; Hata *et al.* 2000; Huang *et al.* 2009; Hesse *et al.* 2010; Masserdotti *et al.* 2010). Among these, the BMP signal-induced binding to SMADs or the transcriptional regulation of an inhibitory SMAD is important for the differentiation of various tissues (Ku *et al.* 2006; Gupta *et al.* 2010; Kamiya *et al.* 2011; Addison *et al.* 2014). Identification of the $L^{rev6\text{-}3}$ mutation in the putative Mad-binding domain raises a possibility that L may also interact with Dpp signaling during development. In addition, our data suggest that the SMAD binding site of Zfp423 family proteins plays an important role in invertebrates as well as vertebrates.

Acknowledgments

We thank Kyung-Ok Cho, Amit Singh, Josh Chern, and Ya-Chieh Hsu for helpful comments on the manuscript and Ya-Chieh Hsu for an initial characterization of *P17* mutation. We are grateful to Aurelio Teleman, Cristina Pallares-Cartes, Ying-Hsuan Wang, and Min-Lang Huang for mutant stocks. We acknowledge the Bloomington Stock Center, *Drosophila* Genomics Resource Center, and Vienna *Drosophila* Resource Center, for fly stocks. This research was supported by the National Research Foundation of Korea (NRF) grants NRF-2014K1A1A2042982, NRF-2016R1A6A3A11935032, and NRF-2017R1A2B3007516 through the Korean Ministry of Education, Science, and Technology.

Literature Cited

Addison, W. N., M. M. Fu, H. X. Yang, Z. Lin, K. Nagano *et al.*, 2014 Direct transcriptional repression of Zfp423 by Zfp521 mediates a bone morphogenic protein-dependent osteoblast *vs.* adipocyte lineage commitment switch. Mol. Cell. Biol. 34: 3076–3085. https://doi.org/10.1128/MCB.00185-14

Alcaraz, W. A., D. A. Gold, E. Raponi, P. M. Gent, D. Concepcion *et al.*, 2006 Zfp423 controls proliferation and differentiation of neural precursors in cerebellar vermis formation. Proc. Natl. Acad. Sci. USA 103: 19424–19429. https://doi.org/10.1073/pnas.0609184103

Awasaki, T., N. Juni, and K. M. Yoshida, 1996 An eye imaginal disc-specific transcriptional enhancer in the long terminal repeat of the tom retrotransposon is responsible for eye morphology mutations of Drosophila ananassae. Mol. Gen. Genet. 251: 161–166.

Bachmann, A., and E. Knust, 2008 The use of P-element transposons to generate transgenic flies. Methods Mol. Biol. 420: 61–77. https://doi.org/10.1007/978-1-59745-583-1_4

Baker, B. S., and K. A. Ridge, 1980 Sex and the single cell. I. On the action of major loci affecting sex determination in Drosophila melanogaster. Genetics 94: 383–423.

Belote, J. M., and B. S. Baker, 1987 Sexual behavior: its genetic control during development and adulthood in Drosophila melanogaster. Proc. Natl. Acad. Sci. USA 84: 8026–8030. https://doi.org/10.1073/pnas.84.22.8026

Bernstein, M., R. A. Lersch, L. Subrahmanyan, and T. W. Cline, 1995 Transposon insertions causing constitutive Sex-lethal activity in Drosophila melanogaster affect Sxl sex-specific transcript splicing. Genetics 139: 631–648.

Bier, E., M. M. Harrison, K. M. O'Connor-Giles, and J. Wildonger, 2018 Advances in engineering the fly genome with the CRISPR-Cas system. Genetics 208: 1–18. https://doi.org/10.1534/genetics.117.1113

Bond, H. M., M. Mesuraca, N. Amodio, T. Mega, V. Agosti *et al.*, 2008 Early hematopoietic zinc finger protein-zinc finger protein 521: a candidate regulator of diverse immature cells. Int. J. Biochem. Cell Biol. 40: 848–854. https://doi.org/10.1016/j.biocel.2007.04.006

Bourque, G., K. H. Burns, M. Gehring, V. Gorbunova, A. Seluanov *et al.*, 2018 Ten things you should know about transposable elements. Genome Biol. 19: 199. https://doi.org/10.1186/s13059-018-1577-z

Brunner, E., D. Brunner, W. Fu, E. Hafen, and K. Basler, 1999 The dominant mutation Glazed is a gain-of-function allele of wingless that, similar to loss of APC, interferes with normal eye development. Dev. Biol. 206: 178–188. https://doi.org/10.1006/dbio.1998.9136

Burns, K. H., and J. D. Boeke, 2012 Human transposon tectonics. Cell 149: 740–752. https://doi.org/10.1016/j.cell.2012.04.019

Chang, H. C., N. M. Solomon, D. A. Wassarman, F. D. Karim, M. Therrien *et al.*, 1995 phyllopod functions in the fate determination of a subset of photoreceptors in Drosophila. Cell 80: 463–472. https://doi.org/10.1016/0092-8674(95)90497-2

Chapman, J. R., M. R. Taylor, and S. J. Boulton, 2012 Playing the end game: DNA double-strand break repair pathway choice. Mol. Cell 47: 497–510. https://doi.org/10.1016/j.molcel.2012.07.029

Chern, J. J., and K. W. Choi, 2002 Lobe mediates Notch signaling to control domain-specific growth in the Drosophila eye disc. Development 129: 4005–4013.

Chuong, E. B., N. C. Elde, and C. Feschotte, 2017 Regulatory activities of transposable elements: from conflicts to benefits. Nat. Rev. Genet. 18: 71–86. https://doi.org/10.1038/nrg.2016.139

Clemmons, A. W., and S. A. Wasserman, 2013 Combinatorial effects of transposable elements on gene expression and phenotypic robustness in Drosophila melanogaster development. G3 (Bethesda) 3: 1531–1538. https://doi.org/10.1534/g3.113.006791

Cook, R. K., S. J. Christensen, J. A. Deal, R. A. Coburn, M. E. Deal *et al.*, 2012 The generation of chromosomal deletions to provide extensive coverage and subdivision of the Drosophila

melanogaster genome. Genome Biol. 13: R21. https://doi.org/10.1186/gb-2012-13-3-r21

Crew, J. R., P. Batterham, and J. A. Pollock, 1997 Developing compound eye in lozenge mutants of Drosophila: lozenge expression in the R7 equivalence group. Dev. Genes Evol. 206: 481–493. https://doi.org/10.1007/s004270050079

Cruz, C., A. Glavic, M. Casado, and J. F. de Celis, 2009 A gain-of-function screen identifying genes required for growth and pattern formation of the Drosophila melanogaster wing. Genetics 183: 1005–1026. https://doi.org/10.1534/genetics.109.107748

Davis, M. B., and R. J. MacIntyre, 1988 A genetic analysis of the alpha-glycerophosphate oxidase locus in Drosophila melanogaster. Genetics 120: 755–766.

Dominguez, M., D. Ferres-Marco, F. J. Gutierrez-Avino, S. A. Speicher, and M. Beneyto, 2004 Growth and specification of the eye are controlled independently by Eyegone and Eyeless in Drosophila melanogaster. Nat. Genet. 36: 31–39. https://doi.org/10.1038/ng1281

Ekas, L. A., G. H. Baeg, M. S. Flaherty, A. Ayala-Camargo, and E. A. Bach, 2006 JAK/STAT signaling promotes regional specification by negatively regulating wingless expression in Drosophila. Development 133: 4721–4729. https://doi.org/10.1242/dev.02675

Evans, C. J., J. M. Olson, K. T. Ngo, E. Kim, N. E. Lee *et al.*, 2009 G-TRACE: rapid Gal4-based cell lineage analysis in Drosophila. Nat. Methods 6: 603–605. https://doi.org/10.1038/nmeth.1356

Filion, G. J., J. G. van Bemmel, U. Braunschweig, W. Talhout, J. Kind *et al.*, 2010 Systematic protein location mapping reveals five principal chromatin types in Drosophila cells. Cell 143: 212–224 [corrigenda: Cell 145**:** 160 (2011)]. https://doi.org/10.1016/j.cell.2010.09.009

Ganko, E. W., C. S. Greene, J. A. Lewis, V. Bhattacharjee, and J. F. McDonald, 2006 LTR retrotransposon-gene associations in Drosophila melanogaster. J. Mol. Evol. 62: 111–120. https://doi.org/10.1007/s00239-004-0312-4

Gorman, M. J., and J. R. Girton, 1992 A genetic analysis of deltex and its interaction with the Notch locus in Drosophila melanogaster. Genetics 131: 99–112.

Gupta, R. K., Z. Arany, P. Seale, R. J. Mepani, L. Ye *et al.*, 2010 Transcriptional control of preadipocyte determination by Zfp423. Nature 464: 619–623. https://doi.org/10.1038/nature08816

Hammonds, A. S., C. A. Bristow, W. W. Fisher, R. Weiszmann, S. Wu *et al.*, 2013 Spatial expression of transcription factors in Drosophila embryonic organ development. Genome Biol. 14: R140. https://doi.org/10.1186/gb-2013-14-12-r140

Hata, A., J. Seoane, G. Lagna, E. Montalvo, A. Hemmati-Brivanlou *et al.*, 2000 OAZ uses distinct DNA- and protein-binding zinc fingers in separate BMP-Smad and Olf signaling pathways. Cell 100: 229–240. https://doi.org/10.1016/S0092-8674(00)81561-5

Hentges, K. E., K. C. Weiser, T. Schountz, L. S. Woodward, H. C. Morse *et al.*, 2005 Evi3, a zinc-finger protein related to EBFAZ, regulates EBF activity in B-cell leukemia. Oncogene 24: 1220–1230. https://doi.org/10.1038/sj.onc.1208243

Hesse, E., H. Saito, R. Kiviranta, D. Correa, K. Yamana *et al.*, 2010 Zfp521 controls bone mass by HDAC3-dependent attenuation of Runx2 activity. J. Cell Biol. 191: 1271–1283. https://doi.org/10.1083/jcb.201009107

Hong, W., M. Nakazawa, Y. Y. Chen, R. Kori, C. R. Vakoc *et al.*, 2005 FOG-1 recruits the NuRD repressor complex to mediate transcriptional repression by GATA-1. EMBO J. 24: 2367–2378. https://doi.org/10.1038/sj.emboj.7600703

Huang, S., J. Laoukili, M. T. Epping, J. Koster, M. Holzel *et al.*, 2009 ZNF423 is critically required for retinoic acid-induced differentiation and is a marker of neuroblastoma outcome. Cancer Cell 15: 328–340. https://doi.org/10.1016/j.ccr.2009.02.023

Jang, C. C., J. L. Chao, N. Jones, L. C. Yao, D. A. Bessarab *et al.*, 2003 Two Pax genes, eye gone and eyeless, act cooperatively in promoting Drosophila eye development. Development 130: 2939–2951. https://doi.org/10.1242/dev.00522

Joyce, E. F., A. Paul, K. E. Chen, N. Tanneti, and K. S. McKim, 2012 Multiple barriers to nonhomologous DNA end joining during meiosis in Drosophila. Genetics 191: 739–746. https://doi.org/10.1534/genetics.112.140996

Kaminker, J. S., C. M. Bergman, B. Kronmiller, J. Carlson, R. Svirskas *et al.*, 2002 The transposable elements of the Drosophila melanogaster euchromatin: a genomics perspective. Genome Biol. 3: RESEARCH0084. https://doi.org/10.1186/gb-2002-3-12-research0084

Kamiya, D., S. Banno, N. Sasai, M. Ohgushi, H. Inomata *et al.*, 2011 Intrinsic transition of embryonic stem-cell differentiation into neural progenitors. Nature 470: 503–509. https://doi.org/10.1038/nature09726

Kankel, M. W., G. D. Hurlbut, G. Upadhyay, V. Yajnik, B. Yedvobnick *et al.*, 2007 Investigating the genetic circuitry of mastermind in Drosophila, a notch signal effector. Genetics 177: 2493–2505. https://doi.org/10.1534/genetics.107.080994

Kapitonov, V. V., and J. Jurka, 2003 Molecular paleontology of transposable elements in the Drosophila melanogaster genome. Proc. Natl. Acad. Sci. USA 100: 6569–6574. https://doi.org/10.1073/pnas.0732024100

Kharchenko, P. V., A. A. Alekseyenko, Y. B. Schwartz, A. Minoda, N. C. Riddle *et al.*, 2011 Comprehensive analysis of the chromatin landscape in Drosophila melanogaster. Nature 471: 480–485. https://doi.org/10.1038/nature09725

Kiviranta, R., K. Yamana, H. Saito, D. K. Ho, J. Laine *et al.*, 2013 Coordinated transcriptional regulation of bone homeostasis by Ebf1 and Zfp521 in both mesenchymal and hematopoietic lineages. J. Exp. Med. 210: 969–985. https://doi.org/10.1084/jem.20121187

Kondo, S., and R. Ueda, 2013 Highly improved gene targeting by germline-specific Cas9 expression in Drosophila. Genetics 195: 715–721. https://doi.org/10.1534/genetics.113.156737

Krattinger, A., N. Gendre, A. Ramaekers, N. Grillenzoni, and R. F. Stocker, 2007 DmOAZ, the unique Drosophila melanogaster OAZ homologue is involved in posterior spiracle development. Dev. Genes Evol. 217: 197–208. https://doi.org/10.1007/s00427-007-0134-7

Ku, M., S. Howard, W. Ni, G. Lagna, and A. Hata, 2006 OAZ regulates bone morphogenetic protein signaling through Smad6 activation. J. Biol. Chem. 281: 5277–5287. https://doi.org/10.1074/jbc.M510004200

Lee, Y. S., and R. W. Carthew, 2003 Making a better RNAi vector for Drosophila: use of intron spacers. Methods 30: 322–329. https://doi.org/10.1016/S1046-2023(03)00051-3

Lindsley, D. L., and G. G. Zimm, 1992 *The Genome of Drosophila melanogaster*. Academic Press, San Diego.

Linheiro, R. S., and C. M. Bergman, 2012 Whole genome resequencing reveals natural target site preferences of transposable elements in Drosophila melanogaster. PLoS One 7: e30008. https://doi.org/10.1371/journal.pone.0030008

Lin, A. C., A. E. Roche, J. Wilk, and E. C. Svensson, 2004 The N termini of Friend of GATA (FOG) proteins define a novel transcriptional repression motif and a superfamily of transcriptional repressors. J. Biol. Chem. 279: 55017–55023. https://doi.org/10.1074/jbc.M411240200

Maksakova, I. A., M. T. Romanish, L. Gagnier, C. A. Dunn, L. N. van de Lagemaat *et al.*, 2006 Retroviral elements and their hosts: insertional mutagenesis in the mouse germ line. PLoS Genet. 2: e2. https://doi.org/10.1371/journal.pgen.0020002

Mao, Z., M. Bozzella, A. Seluanov, and V. Gorbunova, 2008 Comparison of nonhomologous end joining and homologous recombination in human cells. DNA Repair (Amst.) 7: 1765–1771. https://doi.org/10.1016/j.dnarep.2008.06.018

Masserdotti, G., A. Badaloni, Y. S. Green, L. Croci, V. Barili *et al.*, 2010 ZFP423 coordinates Notch and bone morphogenetic protein signaling, selectively up-regulating Hes5 gene expression. J. Biol. Chem. 285: 30814–30824. https://doi.org/10.1074/jbc.M110.142869

Matsubara, E., I. Sakai, J. Yamanouchi, H. Fujiwara, Y. Yakushijin *et al.*, 2009 The role of zinc finger protein 521/early hematopoietic zinc finger protein in erythroid cell differentiation. J. Biol. Chem. 284: 3480–3487. https://doi.org/10.1074/jbc.M805874200

Miller, W. J., and P. Capy, 2004 Mobile genetic elements as natural tools for genome evolution. Methods Mol. Biol. 260: 1–20. https://doi.org/10.1385/1-59259-755-6:001

Morgan, H. D., H. G. Sutherland, D. I. Martin, and E. Whitelaw, 1999 Epigenetic inheritance at the agouti locus in the mouse. Nat. Genet. 23: 314–318. https://doi.org/10.1038/15490

Mozer, B. A., 2001 Dominant Drop mutants are gain-of-function alleles of the muscle segment homeobox gene (msh) whose overexpression leads to the arrest of eye development. Dev. Biol. 233: 380–393. https://doi.org/10.1006/dbio.2001.0229

Nègre, N., C. D. Brown, P. K. Shah, P. Kheradpour, C. A. Morrison *et al.*, 2010 A comprehensive map of insulator elements for the Drosophila genome. PLoS Genet. 6: e1000814. https://doi.org/10.1371/journal.pgen.1000814

Nègre, N., C. D. Brown, L. Ma, C. A. Bristow, S. W. Miller *et al.*, 2011 A cis-regulatory map of the Drosophila genome. Nature 471: 527–531. https://doi.org/10.1038/nature09990

Ong-Abdullah, M., J. M. Ordway, N. Jiang, S. E. Ooi, S. Y. Kok *et al.*, 2015 Loss of Karma transposon methylation underlies the mantled somaclonal variant of oil palm. Nature 525: 533–537. https://doi.org/10.1038/nature15365

Pallares-Cartes, C., G. Cakan-Akdogan, and A. A. Teleman, 2012 Tissue-specific coupling between insulin/IGF and TORC1 signaling via PRAS40 in Drosophila. Dev. Cell 22: 172–182. https://doi.org/10.1016/j.devcel.2011.10.029

Parks, A. L., K. R. Cook, M. Belvin, N. A. Dompe, R. Fawcett *et al.*, 2004 Systematic generation of high-resolution deletion coverage of the Drosophila melanogaster genome. Nat. Genet. 36: 288–292. https://doi.org/10.1038/ng1312

Patel, N. H., 1994 Imaging neuronal subsets and other cell types in whole-mount Drosophila embryos and larvae using antibody probes. Methods Cell Biol. 44: 445–487. https://doi.org/10.1016/S0091-679X(08)60927-9

Port, F., H. M. Chen, T. Lee, and S. L. Bullock, 2014 Optimized CRISPR/Cas tools for efficient germline and somatic genome engineering in Drosophila. Proc. Natl. Acad. Sci. USA 111: E2967–E2976. https://doi.org/10.1073/pnas.1405500111

Port, F., N. Muschalik, and S. L. Bullock, 2015 Systematic evaluation of Drosophila CRISPR tools reveals safe and robust alternatives to autonomous gene drives in basic research. G3 (Bethesda) 5: 1493–1502. https://doi.org/10.1534/g3.115.019083

Potter, C. J., and L. Luo, 2010 Splinkerette PCR for mapping transposable elements in Drosophila. PLoS One 5: e10168. https://doi.org/10.1371/journal.pone.0010168

Prout, M., Z. Damania, J. Soong, D. Fristrom, and J. W. Fristrom, 1997 Autosomal mutations affecting adhesion between wing surfaces in Drosophila melanogaster. Genetics 146: 275–285.

Roy, S., J. Ernst, P. V. Kharchenko, P. Kheradpour, N. Negre *et al.*, 2010 Identification of functional elements and regulatory circuits by Drosophila modENCODE. Science 330: 1787–1797. https://doi.org/10.1126/science.1198374

Ryder, E., F. Blows, M. Ashburner, R. Bautista-Llacer, D. Coulson *et al.*, 2004 The DrosDel collection: a set of P-element insertions for generating custom chromosomal aberrations in Drosophila melanogaster. Genetics 167: 797–813. https://doi.org/10.1534/genetics.104.026658

Ryder, E., M. Ashburner, R. Bautista-Llacer, J. Drummond, J. Webster *et al.*, 2007 The DrosDel deletion collection: a Drosophila genomewide chromosomal deficiency resource. Genetics 177: 615–629. https://doi.org/10.1534/genetics.107.076216

Sancak, Y., C. C. Thoreen, T. R. Peterson, R. A. Lindquist, S. A. Kang *et al.*, 2007 PRAS40 is an insulin-regulated inhibitor of the mTORC1 protein kinase. Mol. Cell 25: 903–915. https://doi.org/10.1016/j.molcel.2007.03.003

Schwartz, Y. B., T. G. Kahn, D. A. Nix, X. Y. Li, R. Bourgon *et al.*, 2006 Genome-wide analysis of Polycomb targets in Drosophila melanogaster. Nat. Genet. 38: 700–705. https://doi.org/10.1038/ng1817

Singh, A., J. Chan, J. J. Chern, and K. W. Choi, 2005 Genetic interaction of Lobe with its modifiers in dorsoventral patterning and growth of the Drosophila eye. Genetics 171: 169–183. https://doi.org/10.1534/genetics.105.044180

Singh, A., X. Shi, and K. W. Choi, 2006 Lobe and Serrate are required for cell survival during early eye development in Drosophila. Development 133: 4771–4781. https://doi.org/10.1242/dev.02686

Spratford, C. M., and J. P. Kumar, 2014 Dissection and immunostaining of imaginal discs from Drosophila melanogaster. J. Vis. Exp. 91:51792. https://doi.org/10.3791/51792

Thibault, S. T., M. A. Singer, W. Y. Miyazaki, B. Milash, N. A. Dompe *et al.*, 2004 A complementary transposon tool kit for Drosophila melanogaster using P and piggyBac. Nat. Genet. 36: 283–287. https://doi.org/10.1038/ng1314

Thurmond, J., J. L. Goodman, V. B. Strelets, H. Attrill, L. S. Gramates *et al.*, 2019 FlyBase 2.0: the next generation. Nucleic Acids Res. 47: D759–D765. https://doi.org/10.1093/nar/gky1003

Tsai, R. Y., and R. R. Reed, 1997 Cloning and functional characterization of Roaz, a zinc finger protein that interacts with O/E-1 to regulate gene expression: implications for olfactory neuronal development. J. Neurosci. 17: 4159–4169. https://doi.org/10.1523/JNEUROSCI.17-11-04159.1997

Vander Haar, E., S. I. Lee, S. Bandhakavi, T. J. Griffin, and D. H. Kim, 2007 Insulin signalling to mTOR mediated by the Akt/PKB substrate PRAS40. Nat. Cell Biol. 9: 316–323. https://doi.org/10.1038/ncb1547

Wang, L. H., S. J. Chiu, and Y. H. Sun, 2008 Temporal switching of regulation and function of eye gone (eyg) in Drosophila eye development. Dev. Biol. 321: 515–527. https://doi.org/10.1016/j.ydbio.2008.06.038

Wang, Y. H., and M. L. Huang, 2009 Reduction of Lobe leads to TORC1 hypoactivation that induces ectopic Jak/STAT signaling to impair Drosophila eye development. Mech. Dev. 126: 781–790. https://doi.org/10.1016/j.mod.2009.08.005

Yao, J. G., and Y. H. Sun, 2005 Eyg and Ey Pax proteins act by distinct transcriptional mechanisms in Drosophila development. EMBO J. 24: 2602–2612. https://doi.org/10.1038/sj.emboj.7600725

Zaboikin, M., T. Zaboikina, C. Freter, and N. Srinivasakumar, 2017 Non-homologous end joining and homology directed DNA repair frequency of double-stranded breaks introduced by genome editing reagents. PLoS One 12: e0169931. https://doi.org/10.1371/journal.pone.0169931

Communicating editor: R. Duronio